General Disclaimer

One or more of the Following Statements may affect this Document

- This document has been reproduced from the best copy furnished by the organizational source. It is being released in the interest of making available as much information as possible.

- This document may contain data, which exceeds the sheet parameters. It was furnished in this condition by the organizational source and is the best copy available.

- This document may contain tone-on-tone or color graphs, charts and/or pictures, which have been reproduced in black and white.

- This document is paginated as submitted by the original source.

- Portions of this document are not fully legible due to the historical nature of some of the material. However, it is the best reproduction available from the original submission.

THE PREDICTION OF SEA-SURFACE TEMPERATURE VARIATIONS BY MEANS OF AN ADVECTIVE MIXED-LAYER OCEAN MODEL

by

Robert M. Atlas

Technical Report
Grant NGR 33-013-086
Goddard Space Flight Center

The City College, CUNY

Contribution No. 69, CUNY Institute of Marine and Atmospheric Science

Table of Contents

List of Figures

List of Figures (continued)

Acknowledgements

The author wishes to thank his advisor, Professor Jerome Spar, for his valuable guidance throughout this work. He also wishes to thank James R. Miller for his advice and suggestions and Robert Jastrow, director of GISS, Milton Halem, William Quirk and Gary Russell of the Goddard Institute for Space Studies for providing facilities and computing services. He is also grateful to the Woods Hole Oceanographic Institution, the U.S. Navy Fleet Numerical Weather Central, and the Marine Section of the National Weather Service in New York City, for providing data for this investigation. Finally, the author would like to thank his wife, Shirley, for her unstinting cooperation and encouragement.

This research was sponsored by the National Aeronautics and Space Administration, Goddard Space Flight Center, under Grant NGR 33-013-086 to the City College of the City University of New York.

Abstract

An advective mixed-layer ocean model has been developed by eliminating the assumption of horizontal homogeneity in an already existing mixed-layer model, and then superimposing a mean and anomalous wind driven current field. This model is based on the principle of conservation of heat and mechanical energy and utilizes a box grid for the advective part of the calculation. Three phases of experimentation have been conducted. In the first phase, the model's ability to account for climatological sea-surface temperature (SST) variations in the cooling and heating seasons was evaluated. These experiments showed that the inclusion of advection results in a large improvement of the model's accuracy and also illustrated the relative importance of advection and mixed-layer depth variations. The second phase of experimentation consisted of a series of sensitivity tests in which the effect of hypothetical anomalous winds was evaluated. These tests showed that sustained highly anomalous winds are capable of generating large-scale SST anomalies. In the third phase of experimentation, a thirty-day synoptic calculation with the model was conducted. For the case studied, the accuracy of the predictions was improved by the inclusion of advection, although non-advective effects appear to have dominated.

1. Introduction

It is well known that the upper layers of the oceans undergo substantial temperature variations and that these variations are primarily brought about by solar and long-wave radiation, heat exchange with the atmosphere and heat transfer within the ocean itself. Despite numerous studies of oceanic heat transfer, there are still conflicting opinions regarding the role of temperature advection and the need for its inclusion in numerical models of the upper ocean.

Namias (1959) was among the first to suggest that anomalous temperature advection in the ocean could be a major cause of large scale sea-surface temperature (SST) anomalies. Utilizing the principle that anomalous winds produce an anomalous drag on the surface water and force an anomalous Ekman drift, he computed surface water displacement vectors by applying Ekman's empirical formula

$$\frac{V_o}{W} = \frac{0.0127}{\sqrt{\sin \phi}} , \qquad (1)$$

to the seasonal anomalous geostrophic wind distribution, where Vo is the speed of the surface water current, W is the surface wind speed and ϕ is the latitude. He then superimposed these displacement vectors on the normal sea-surface temperature field in order to compute simple advective changes. These advectively computed SST anomalies were then compared with

the observed anomalies. Although only slight agreement between the two fields could be seen, Namias was able to conclude that advection does contribute to the formation of SST anomalies but that in this case, other factors must have been dominant. He also suggested that anomalous winds could produce anomalous upwelling, downwelling and air-sea heat exchange. However, no attempt was made to determine the relative importance of each.

Following this early work of Namias, Eber (1961) used monthly rather than seasonal wind anomalies and the SST fields for the months being studied instead of long-term normals. For the same data period as Namias (1959), he found a much closer agreement between the advectively computed SST anomalies and the observed anomalies for the winter case, while for the fall case he found only a slight agreement. This led him to conclude that advection was the dominant factor for the winter studied although other factors must have dominated during the fall. He then suggested that seasonal variations of the thermal structure in the wind-mixed layer might be significant but did not attempt to evaluate its effect.

Subsequent empirical studies by Namias (1969, 1970, 1971, 1972, 1973, 1974) have added further credence to the idea that advection within the oceans can be a major cause of SST variations, and therefore the generation of large-scale

SST anomalies. In a study of large-scale variations in sea-surface temperatures in the North Pacific, Namias (1970) illustrated how water masses could be transported around the North Pacific gyre and how anomalous winds or currents could affect this transport. In 1953 the zonal westerlies were stronger than normal and the torque on the Pacific gyre was increased, while in 1963 the zonal westerlies and sub-tropical easterlies were much weaker than normal and the torque on the Pacific gyre was greatly decreased. (This torque was actually reversed during the winter of 1963.) Namias linked these anomalous winds to the large scale SST anomalies of these years and also presented correlations of the zonal wind and sea-surface temperatures with season. A strong negative correlation was noted for the winter case.

In his evaluation of the physical causes of the winter 1971-1972 SST anomalies, Namias (1972) presented diagnostic computations of the anomalous air-sea heat exchange which occurred during this period. These values revealed that anomalous heat exchange could not have produced the observed anomalous SST variations and that other factors such as advection and mixed-layer depth changes must have been dominant. However, as noted by Namias (1972), there was insufficient data to evaluate the effects of changes in the mixed-layer depth.

As a result of these empirical studies by Namias and those of Bjerknes (1966, 1969), the role of the oceans as a lower boundary in atmospheric prediction models has received greater emphasis and it has become increasingly important to predict SST variations accurately. Atmospheric response to SST anomalies is one of the major problems of meteorology today and it is generally accepted that accurate long-range weather forecasting is not possible unless SST variations can also be predicted.

Initial attempts at extended and long-range numerical weather prediction utilized models in which the SST field was specified climatologically and did not vary with time. A series of experiments in which SST anomalies were superimposed on the climatoligical SST fields, was conducted independently by Rowntree (1972), Spar (1973), and Houghton, et al. (1974), to determine the influence of large-scale SST anomalies in such atmospheric general circulation models. These experiments showed that the model atmosphere is indeed sensitive to large, persistent SST anomalies, and that remote as well as local effects can be significant.

Later experiments by Spar and Atlas (1975) and Spar, Atlas and Kuo (1975), in which synoptic rather than climatological SST fields were specified in an atmospheric model, indicated that the use of specified synoptic SST data or the

daily updating of such fields does not necessarily result in an improvement of the atmospheric predictions. This is partially due to the loss of predictability in such models (Sommerville et al. 1974, Druyan et al. 1975, Seidman 1975) and the poor quality of synoptic SST data (Saur 1963, Rao et al. 1972, Jastrow and Halem 1973, Smith et al. 1974, Rao 1974).

Despite these somewhat negative results, the prediction of SST variations remains as one of the most important problems in long-range weather forecasting, and such predictions would no doubt benefit the maritime and fishing industries as well. Although empirical methods have been devised (Namias 1968, 1969, 1972, 1973, Hammond 1974) to utilize SST predictions for long-range forecasting, the major thrust of recent research has been to develop predictive ocean models which could be coupled to atmospheric general circulation models. The predictions for both the atmosphere and oceans could then be carried out simultaneously, allowing the predicted changes in each medium to affect the other. It would thus be possible to study the complex interactions which result from anomalies in both the atmosphere and ocean.

The purpose of this particular study is to develop an advective mixed-layer ocean model by incorporating the effects of horizontal temperature advection into an already

existing mixed-layer model, and then to study the role of temperature advection in the prediction of sea-surface temperature variations. While this model was designed for the purpose of eventually coupling it to an atmospheric model, no attempt has been made to do the coupling in this study. Instead this study will serve to demonstrate the effect of advection by mean ocean currents and indicate how anomalies in the atmospheric circulation can result in SST variations. This latter point should be extremely important for predictive runs as well as for simulation studies with coupled atmosphere-ocean models.

Specific objectives of this research are to determine (1) if advective effects are significant within the mixed-layer ocean model, (2) if the inclusion of advection results in an improvement in the accuracy of the SST predictions, (3) for which regions (and times) advective effects are most important, (4) the relative importance of advection and mixed-layer deepening in predicting sea-surface temperature changes, and (5) the effect of anomalous wind-generated ocean currents on the development and maintenance of SST anomalies within the model. In order to carry out these objectives, the advective scheme must include the advective effects of anomalous wind-generated currents as well as mean ocean currents.

After a brief review of ocean modeling, the development of the advective mixed-layer ocean model and results of experimentation with this model will be presented. Three phases of experimentation were conducted in order to carry out the above objectives. These consisted of: (1) climatological simulation, in which the model's ability to predict climatological SST variations was evaluated, (2) sensitivity tests, in which the effect of anomalous winds was determined, and (3) a synoptic calculation, in which an attempt was made to predict the observed thirty day SST change from January 1 to January 31, 1974.

2. Review of Ocean Models

2.1 Background

As stated by Miller (1973), there are two primary approaches to the development of ocean models suitable for coupling to atmospheric models. The first of these is the development of baroclinic models of the entire (three-dimensional) ocean which are based on the principles of conservation of mass, momentum, energy, heat, and salt. In these models, the finite difference approximations to the Navier-Stokes system of equations (Bryan 1975) are simplified by assuming that (1) density differences in the ocean are negligible in comparison with the mean density, and therefore the mean density can be substituted for the actual density everywhere but in the buoyancy term (the Boussinesq approximation), (2) the vertical scale in the ocean is much smaller than the horizontal scale, and therefore the vertical acceleration terms are negligible in comparison with the buoyancy term, (3) molecular viscosity is negligible, (4) the depth of the ocean is small in comparison with the earth's radius, and (5) the angular velocity of the ocean's motion is much smaller than the earth's angular velocity. Various other simplifying assumptions are included depending on the particular model.

In recent years, a number of such general ocean circulation models (Bryan 1969, 1975, Cox 1975, Takano 1975) have been developed. While models of this type are desirable for the study of oceanic processes and indeed necessary for the long-term integrations of climatic studies, they in general do not adequately resolve the upper layer of the oceans and also have very long response times when coupled with atmospheric models. The second approach to ocean modeling is to model the active upper layer of the oceans only. Since these models have short response times when coupled with atmospheric models, they are considered to be preferable for short and medium-range predictions.

Two basic approaches to modeling the upper ocean exist. The first approach is to account for SST changes wholly in terms of radiation, heat exchange with the atmosphere, and heat transfer within the oceans. These models are either two or three-dimensional in character and do not account for temperature changes due to mixed-layer deepening or the formation of new mixed layers (i.e. The mixed-layer depth does not vary with time). The second approach is to develop a model which is capable of predicting mixed-layer depth changes. Models of this type are generally one-dimensional in nature and therefore do not adequately account for horizontal heat transfer processes within the oceans.

2.2 Models With Constant Mixed-Layer Depth

All of the models of this type, to be discussed herein, are based primarily on the application of the thermodynamic energy equation to the upper layer of the ocean and utilize Ekman's empirical formula (1) to relate drift currents in the upper ocean to the low level atmospheric winds. As mentioned earlier, Namias (1959) was among the first to apply Ekman's formula (1) in an empirical study of SST anomalies. His model assumed that anomalous SST changes resulted entirely from anomalous horizontal advection and therefore,

$$\frac{\partial T_s}{\partial t} = -\mathbf{V}_a \cdot \nabla T_m \,, \qquad (2)$$

where Ts is the ambient sea-surface temperature, Tm represents the climatological mean sea-surface temperature, ∇ is the horizontal gradient operator (∇Tm is the horizontal mean temperature gradient), and $\mathbf{V}_a$ refers to the anomalous current velocity derived from the use of (1). Since this model explicitly neglects all heat sources and sinks, it is not suitable for realistic prediction of the SST field.

Arthur (1966) suggested that an additional advection term, representing the advection of anomalous isotherms by the mean monthly surface currents be included in this

model. Jacob (1967) incorporated this second advection term and an anomalous heating term (derived from empirical formulas), into Namias' model and performed his calculations over a constant mixed-layer depth of 50 meters throughout his grid. These experiments indicated that the inclusion of these terms resulted in a significant improvement in the SST predictions for a two week to one month period. However Jacobs' model was not able to account for all of the large SST anomalies which were observed.

Adem (1970) developed a model for the entire Northern Hemisphere (with the exception of the Indian Ocean) which was based on the application of the principle of conservation of mass as well as the thermodynamic energy equation. His model included mean and anomalous advection, horizontal turbulent diffusion, heat sources and sinks and vertical exchange between the upper ocean and the region below the thermocline. He assumed that the mixed-layer depth was constant at either 50 or 100 meters and performed his calculations for both values. His experiments demonstrated the usefulness of applying mean and wind drift currents to the SST field in order to account for advection as well as the relative importance of horizontal temperature advection in this model.

Clark (1972) performed experiments with a model which included heat source and sink terms and anomalous

advection only. He computed SST anomalies that would result from the inclusion of only advection, evaporative heat exchange, or total surface heat exchange individually. These experiments showed that the advectively computed SST anomalies are closely related to atmospheric pressure anomalies and that anomalous advection can be an important factor in bringing about anomalous SST variations. However, as indicated earlier by Eber (1961) and Namias (1972), and as stated by Clark (1972) the omission of mixed-layer depth changes in these calculations is a serious deficiency and therefore such changes should be included in any predictive model or specification procedure for SST variations.

2.3 The Development of Mixed-Layer Models

Although predictive models of the wind-mixed layer are relatively recent in origin, attempts to model and/or describe mixed-layer depth changes have been going on since Ekman's (1905) study of the influence of the earth's rotation on ocean currents. Ekman assumed that the water was homogeneous and applied a constant value of the eddy viscosity coefficient to obtain his famous "spiral" calculation. This "spiral" concept therefore did not contain a well mixed upper layer bounded by a distinct gradient below.

However, Ekman realized that his theory was an oversimplification and stated that the coefficient of eddy viscosity cannot be constant when the density of the water is not uniform (as is the case in the real ocean).

Munk and Anderson (1948) developed a density stratified model of the upper ocean utilizing eddy coefficients of viscosity and conductivity which varied with depth. They obtained a steady state (non-time dependent) solution for the distribution of temperature and velocity with depth which accounted for the upper mixed layer and the thermocline below. However, their computations yielded thermocline depths which were in general less than half of the observed depths and they were only able to apply their theory where evaporation was small, the heat flux was positive, and advection was negligible.

Other steady state models of the thermocline have been developed by Kitaigorodski in 1960 and Kraus and Rooth in 1961 (see Kraus and Turner, 1967). Kitaigorodski computed the depth of the mixed layer from the balance between the mean work of the wind stress and the work required to mix incoming heat downward, while Kraus and Rooth showed how the absorption of heat through a finite depth in conjunction with a net heat loss at the surface (through evaporation, conduction, and long-wave radiation) resulted in convection within the mixed layer. In recent years several time-dependent,

one-dimensional mixed-layer ocean models have been developed for the purpose of short and medium-range SST prediction. These models which are primarily based on the conservation of heat and mechanical energy, as well as suitable boundary conditions, provide reasonable predictions for the changes in mixed-layer depth and sea-surface temperature. But because of the assumption of a horizontally homogeneous ocean in these models and their one-dimensional nature, they neglect or do not adequately take account of important dynamical effects such as advection of heat by horizontal ocean currents and upwelling and downwelling.

The first realistic time-dependent model of the seasonal thermocline was developed by Kraus and Turner (1967). They assumed that heat fluxes into the mixed layer and mass entrained at the bottom of the layer are instantaneously mixed uniformly throughout the layer, and thereby considered the mixed layer to be vertically homogeneous. As a result of this assumption, it was not necessary for them to utilize eddy coefficients in their formulation. For the case of constant mixing by light winds (approximately equal to 5 meters per second), they were able to obtain quantitative as well as qualitative predictions for variations in sea-surface temperature and mixed-layer depth. It was found that their model's predictions agree reasonably well with oceanic observations and with earlier laboratory experiments (Turner and Kraus 1967).

In a subsequent laboratory experiment, Kato and Phillips (1969) studied the development of a mixed layer in an annular tank. They applied a constant stress to the surface of an initially quiescent fluid with a uniform density gradient, and observed the growth of a turbulent layer by entrainment of the underlying fluid. It was found that the rate of increase of the potential energy of the stratified fluid is proportional to the rate of dissipation of kinetic energy in the turbulent layer, and that the thickness of this turbulent layer increased as the time to the one-third power. Kato and Phillips reasoned that these results should be directly applicable to the real ocean.

Denman (1973) developed a time-dependent, one-dimensional model of the upper ocean, which is essentially a generalization of the Kraus and Turner model and is consistent with the results of Kato and Phillips. This model assumes that the ocean is a stably stratified, incompressible fluid obeying the Boussinesq approximation, and it ignores wave-induced dynamical effects. The ocean is considered to be horizontally homogeneous except that indirect effects can result from the non-zero curl of the wind stress.

Figure 1. illustrates the fundamental parameters and boundary conditions of the Denman model. From this figure, it can be seen that the vertically homogeneous mixed layer is

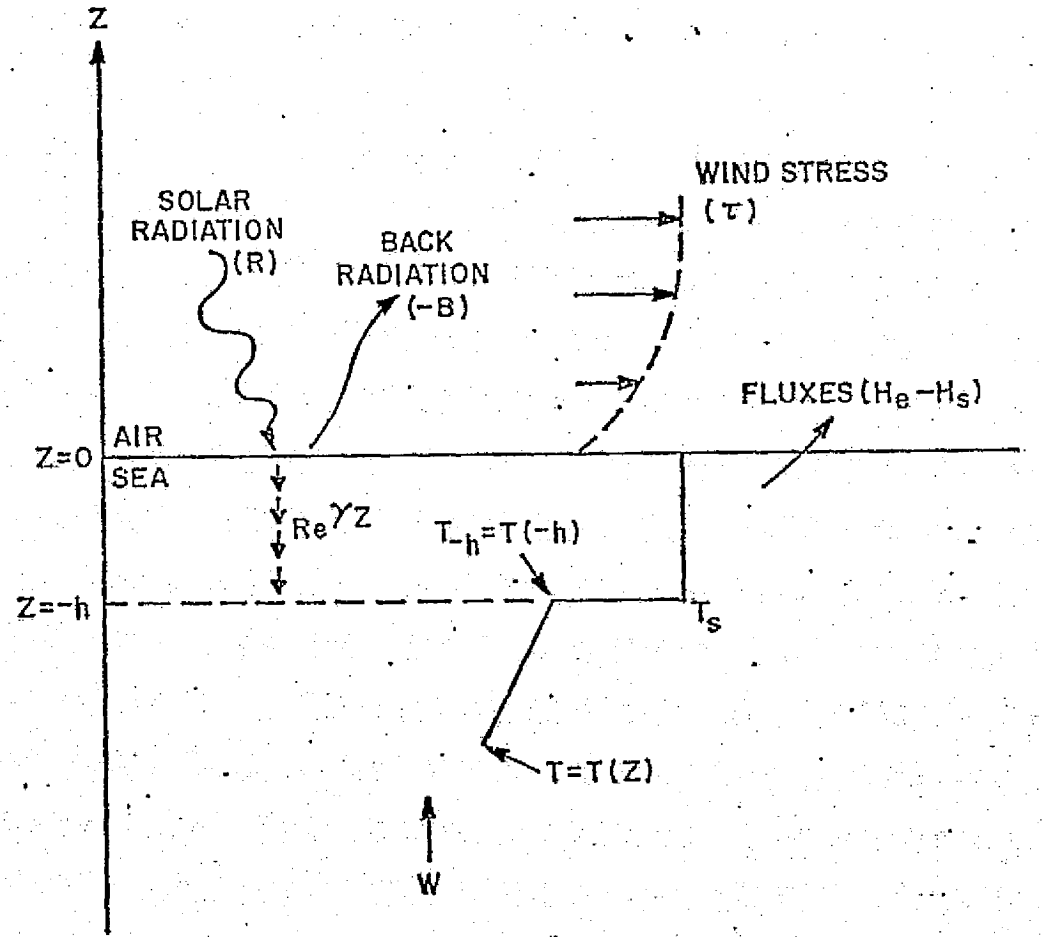

Fig. 1. Schematic illustration of the vertical temperature profile and the boundary inputs assumed in the Denman model (after Denman 1973).

bounded on the bottom by a temperature discontinuity, below which a climatological temperature gradient is specified. The vertical temperature profile may be specified therefore in terms of three variables: T_s (the temperature of the mixed layer), T_{-h} (the temperature immediately below the mixed layer), and h (the mixed-layer depth).

From the conservation equations for thermal and mechanical energy, Denman derived the following set of three first order ordinary differential equations for the prediction of these variables:

$$\frac{dT_s}{dt} = \frac{2}{h^2}\left[-(G-D)+h(B+H_e+H_s)+R(h-\gamma^{-1}+\gamma^{-1}e^{-\gamma h}\right], \quad (3)$$

$$H\left[w+\frac{dh}{dt}\right] = \frac{2\left[G-D+R\gamma^{-1}(1-e^{-\gamma h})\right]-h\left[B+H_e+H_s+R(1+e^{-\gamma h})\right]}{h(T_s-T_{-h})}, \quad (4)$$

$$\frac{d}{dt}T_{-h} = \gamma R_e{}^{-\gamma h}-(w+dh/dt)\left.\frac{\partial T}{\partial z}\right|_{-h} . \quad (5)$$

In the above equations, G represents the production of turbulent energy from the wind stress at the sea surface, D is the total energy dissipation within the mixed layer, γ is an average extinction coefficient for solar radiation, w is an imposed vertical velocity at the bottom of the layer, and H is a Heaviside step function which is equal to zero if $w + dh/dt \leq 0$ or one if $w + dh/dt > 0$. The terms B, He, Hs

and R represent the surface fluxes of the net long-wave radiation, latent heat, sensible heat, and short-wave solar radiation, all divided by ρc_p where ρ and c_p are the density and specific heat of sea water respectively, i.e.

$$(R,\ B,\ H_e,\ H_s) = \frac{1}{\rho c_p}\ (R^*,\ B^*,\ H_e^*,\ H_s^*)$$

where the * denotes that these fluxes are at the sea surface.

The set of coupled equations (3-5) is similar to the predictive equations of Kraus and Turner's (1967) model. However, Kraus and Turner solved their model analytically on a time scale of months whereas this model is solved numerically on a time scale of days. Because of this, the boundary conditions for the Denman model have been formulated somewhat more precisely. Specifically, the Denman model includes a specified temperature gradient below the temperature discontinuity and allows the penetration of solar radiation into this region.

Obviously the predictions of the above system of equations depend very strongly on the value of the Heaviside step function H. If H = 1, then the model is in a wind dominated regime and the entrainment mixing term (w + dh/dt) is included in (4). Under these conditions, the mixed layer is deepening and cold water from below the temperature discontinuity will be entrained into the mixed layer due to the

work done by turbulence against the buoyancy. The temperature of the mixed layer would tend to decrease due to this effect.

When H = 0, the model is in a heat-dominated regime and there is no entrainment mixing term in (4). Since the absorption of solar radiation is greatest near the surface of the ocean and all of the available turbulent energy from the wind stress must be used to redistribute this heat uniformly throughout the mixed layer, none of the energy is available to deepen the mixed layer further. Therefore, in this case, the mixed-layer depth will remain unchanged or under conditions of rapid heating and low winds, a new shallower mixed layer of warmer water will form. This new mixed layer would be superimposed on the old temperature profile and there would thus be more than one temperature discontinuity in the profile.

Denman performed a number of experiments with this model for both the wind-dominated and heat-dominated regimes. For the wind-dominated case, he found that (1) doubling the turbulent energy available for mixing over a two day period, produced a significant increase (almost 30%) in the mixed-layer depth, (2) decreasing the stratification in the model to one half of its original value resulted in a smaller but still important effect on mixed-layer depth, (3) typical

summer heating rates (solar radiation of 400 cal. cm.$^{-2}$ day^{-1} coupled with back radiation of -80 cal. cm.$^{-2}$ day^{-1}) did not significantly affect the mixed-layer depth, and (4) large evaporative heat losses (typical of winter conditions) coupled with high winds cause strong convective mixing which does have an important effect on the mixed layer. For the heat dominated case, he found that the predictions of the model are sensitive to the value of the extinction coefficient and that decreasing this extinction coefficient to one half of its original value increases the mixed-layer depth significantly (70% in the case studied). He also found that if the extinction term was not retained in the region below the mixed layer, that the mixed-layer depth was overestimated by 15%.

Denman and Miyake (1973) utilized the Denman model to predict SST and mixed-layer depth changes at Ocean Station Papa during a twelve day period from 13 to 24 June, 1970. Oceanographic observations, described in their paper, indicate that during the summer, sensible and latent heat fluxes, horizontal temperature advection, and vertical advection from below the mixed layer may all be neglected at this location (50 N, 145 W) in the Pacific Ocean. Under these conditions, the formation of a shallow mixed layer of warm water is caused primarily by intense solar radiation and low wind speeds.

Deepening of the layer is induced primarily by the increased winds accompanying atmospheric storms. For this period the Denman model's predictions of SST agreed well with observations and the model's profiles did simulate the time-dependent behavior of the mixed-layer.

Two other one-dimensional models have been developed to predict SST variations and to explain the time-dependent behavior of the mixed-layer. Pollard, Rhines and Thompson (1973) developed a model, which like Denman's, describes the response of the upper ocean to an imposed wind stress and heat flux. In the Denman model, part of the available turbulent energy from the wind stress induces a slow erosion of the stably stratified, quiescent layer below the mixed layer. However, in the Pollard, Rhines and Thompson model, available turbulent energy is used to drive inertial motions within the mixed layer. These motions allow for a more rapid erosion of the stably stratified layer and therefore a more rapid mixed-layer deepening. Niiler (1973) has developed a model which includes both of these erosion mechanisms. He states that both of these processes are important at different times. However the necessity for including inertial motions for SST prediction is not well established.

As previously mentioned, there has been a major effort in recent years to develop coupled atmosphere-ocean

models, and for short and extended-range prediction, it is desirable to utilize a model of the upper ocean for this purpose. At the Goddard Institute for Space Studies (GISS), the one dimensional mixed-layer ocean model developed by Denmán has been adapted for global use in conjunction with the GISS atmospheric model by Miller (1974). This GISS ocean model has a horizontal grid spacing of 4^{o} in latitude and 5^{o} in longitude. Despite the fact that this is a global grid, the one-dimensional nature of the Denman model has not changed and the predictions at each point are carried out independently. Some modifications to the original Denman model have been made by Miller in order to improve the SST and mixed-layer depth predictions. These will be discussed briefly in the next sections.

As a result of the initial experimentation with this GISS ocean model and for the purposes listed in the introduction, an advective mixed-layer ocean model has been developed by incorporating advective effects into this model. In order to account for the horizontal advection of heat at each gridpoint, the assumption of a horizontally homogeneous temperature field for the entire ocean has been eliminated (thus allowing for horizontal temperature gradients) and a mean and anomalous wind driven current field has been superimposed on the grid. By taking this approach we still

allow the modified Denman model to account for the effects of solar and back radiation, sensible and latent heat exchange with the atmosphere, and mixed-layer depth changes at each point, while the superimposed current field serves to couple the gridpoints through the advection of heat and mass.

3. Description of the Advective Mixed-Layer Model

3.1 Basic Theory

With the exception of the advection scheme, the model to be described herein is almost identical to the Denman model and therefore our approach will be very similar. As in the Denman model, we assume that the ocean is a stably stratified, incompressible, fluid obeying the Boussinesq approximation and ignore wave induced dynamical effects, molecular heat fluxes and the viscous generation of heat. We do not however, assume that the entire ocean is horizontally homogeneous in all properties at this time. Thus our derivation will include horizontal advection terms for heat and mass. Horizontal turbulent diffusion will be assumed to be negligible when compared to the other heat exchange processes (Clark 1972) and will not be included. It can be argued (Bathen 1971) that lateral diffusion is important in certain regions. Although this is probably true, these effects will not be considered here.

Figure 1 depicts the main parameters and processes of the Denman model. The GISS ocean model profile is only slightly different from this and is depicted in four forms in Figure 2.

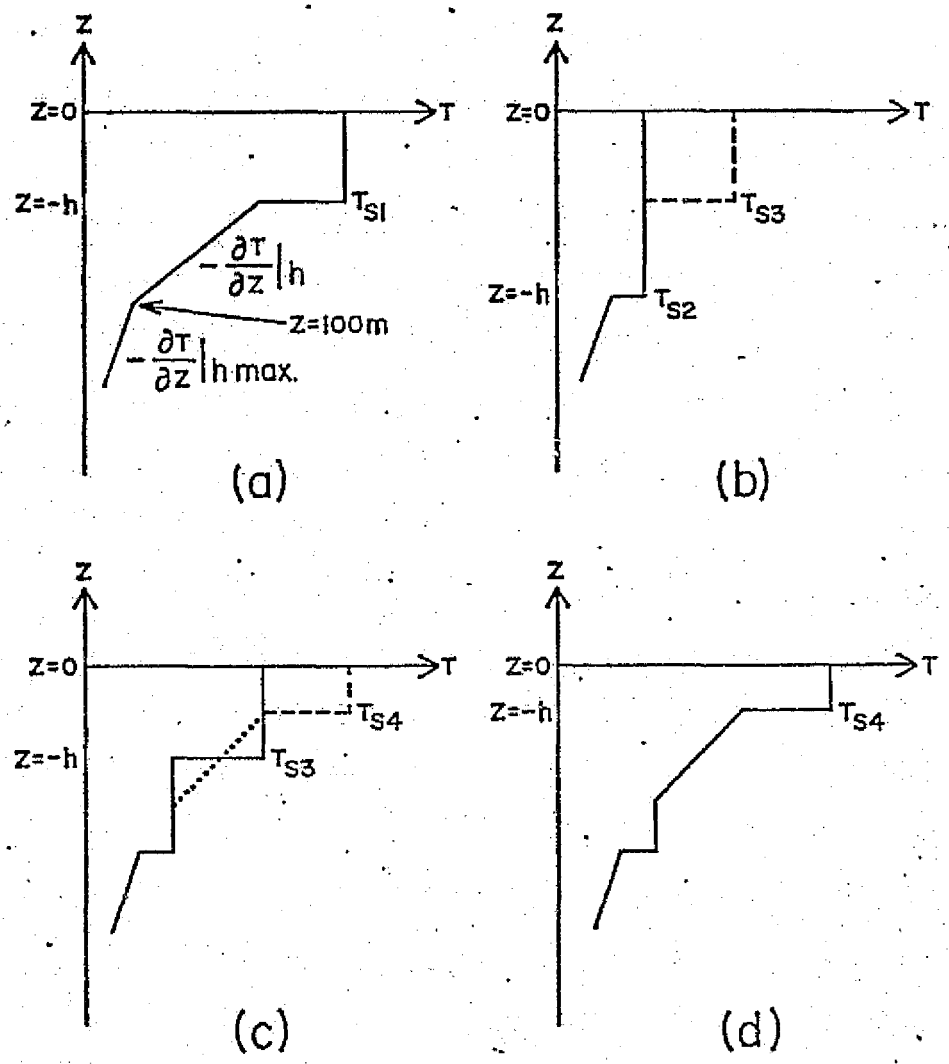

Fig. 2. Schematic illustration of the vertical temperature profile of the GISS ocean model at four different stages of development. (a) Initial profile. (b) Typical profile at end of cooling season. (c) Typical profile at beginning of heating regime. (d) Typical profile during the heating season. $T_{s1}>T_{s2}$ and $T_{s4}>T_{s3}>T_{s2}$.

When the model is initialized, the initial temperature profile at a gridpoint will be similar to that shown in Figure 2a. This structure consists of a vertically homogeneous mixed layer bounded by a temperature discontinuity, below which two temperature gradients are specified. The upper temperature gradient $\frac{\partial T}{\partial z}\Big|_h$ corresponds to the seasonal thermocline while the lower one $\frac{\partial T}{\partial z}\Big|_{h\ max}$ corresponds to the temperature gradient below 100 meters. This structure is somewhat more realistic than Denman's for modeling an entire cooling season.

During the cooling season the mixed layer deepens, and by the end of this season the mixed-layer depth is generally between 100 and 200 meters in mid latitudes (Miller 1974). The solid line in Figure 2b represents a typical profile at the end of the cooling season (Miller 1974). The deepening of the mixed layer is arbitrarily cut off at a maximum depth of 200 meters. If this point is reached, then the mixed layer continues to cool until the temperature jump at the bottom goes to zero or a heating regime begins. When the heating regime begins, a new (shallower) mixed layer forms at the surface and this is superimposed on the preceding temperature profile. In this case, there is a new isothermal layer and temperature discontinuity (as shown by the dashed line in Figure 2b). The temperature gradient immediately below this is initially set equal to the remaining portion of

the old isothermal layer (i.e. $\frac{\partial T}{\partial z}\Big|_h = 0$, initially). The initial heating regime profile that would result from this is represented by the solid line in Figure 2c. As the heating regime continues a shallower mixed layer forms and this new layer is superimposed on the preceding profile. This is illustrated by the dashed line in Figure 2c. At this stage, the profile is geometrically adjusted to assure that there are equal areas of warming and cooling on each side of the upper temperature discontinuity. This eliminates this temperature discontinuity and yields a new temperature gradient $\frac{\partial T}{\partial z}\Big|_h$, as illustrated by the dotted line in Figure 2c. The complete profile which would result from this process is depicted in Figure 2d.

The advective model's profile is exactly the same as that described above except that horizontal ocean currents are included in the mixed layer. These currents are averaged within the mixed layer, and for simplicity it is assumed that the current speed goes to zero at the bottom of the mixed layer.

3.2 Model Equations

Following Denman (1973) the thermodynamic energy equation for the ocean may be written as

$$dT/dt = Q_T/\rho c_p \qquad (6)$$

where T is the temperature and Q_T is the heat source, due to absorption of solar radiation. Denman (1973) makes the assumption that $Q_T = \gamma R_* e^{\gamma z}$, where z is the negative depth in the ocean. If we substitute this expression into the time averaged, Eulerian, turbulent form of (6) we obtain

$$\underset{(1)}{\frac{\partial T}{\partial t}} + \underset{(2)}{\bar{V} \cdot \nabla T} + \underset{(3)}{\frac{\partial}{\partial z}(\overline{w'T'})} = \frac{\gamma R_* e^{\gamma z}}{\rho c_p} , \qquad (7)$$

where $\bar{V}$ is the horizontal current velocity and the primes in this and the following equations denote perturbation quantities, i.e. deviations from local, climatological mean values. Term 1 is the local change of temperature, term 2 represents the horizontal temperature advection by ocean currents, and term 3 is the local divergence of turbulent heat flux. In this equation, the vertical temperature advection term $w\frac{\partial T}{\partial z}$ has been eliminated because of the absence of vertical temperature gradients within the mixed layer, and horizontal eddy diffusion has been neglected.

Denman (1973) employs Phillips (1966) turbulent kinetic energy equation,

$$\frac{\partial}{\partial t}\left(\frac{\overline{c^2}}{2}\right) = -\overline{s'w'}\frac{\partial S}{\partial z} - \frac{\partial}{\partial z}\left[w'\left(\frac{p'}{\rho_o} + \frac{c^2}{2}\right)\right] - \frac{\overline{w'\rho'}g}{\rho_o} - \varepsilon \quad , \qquad (8)$$

(1) (2) (3) (4)

where c^2 represents the eddy kinetic energy, S represents the mean horizontal current in the mixed layer, P denotes pressure, g is the gravitational acceleration, and ε represents the rate of dissipation of turbulent energy. This equation is used without modification in the advective model on the assumption that the horizontal advection of kinetic energy is negligible.

In equation 8, term 1 represents the time rate of change of kinetic energy of the turbulent motion, which according to Denman (1973), is negligibly small. Term 2 represents the rate of production of turbulent energy by the turbulent Reynolds stresses, which act on the mean current shear. Term 3 is the local divergence of the vertical transport of turbulent mechanical energy. (It is this term which serves to instantly mix the turbulent energy uniformly throughout the layer.) Term 4 is the rate of turbulent energy loss, due to work done against the lower density gradient. The elimination of term 1 results in a steady state relationship, expressing the balance between energy source and sink terms. Thus the steady state mechanical energy equation for the

turbulent motion is

$$-\overline{s'w'}\,\frac{\partial S}{\partial Z}-\frac{\partial}{\partial Z}\left[w'\left(\frac{p'}{\rho_o}+\frac{c^2}{2}\right)\right]=\alpha g\overline{w'T'}+\varepsilon \qquad (9)$$

It is now necessary to consider the application of the principles of conservation of heat and mechanical energy (equations 7 and 9) to the mixed layer, the interface below the mixed layer, and the region below this interface. Although Figures 1 and 2 depict an artificial temperature discontinuity at $Z=-h$ it is more reasonable to consider the interface between the mixed layer and lower layer as having some thickness Δh. This is illustrated in Figure 3, which is taken directly from Denman's (1973) paper.

Denman (1973) evaluates the mixing entrainment at the bottom of the mixed layer ($\overline{w'T'}\big|_{-h}$) by integrating the thermodynamic energy equation across the interface

$$\int_{-h}^{-h+\Delta h}\left[\frac{\partial T}{\partial t}+\mathbf{V}\cdot\nabla T+w\frac{\partial T}{\partial Z}+\frac{\partial}{\partial Z}\left(\overline{w'T'}\right)\right]=\int_{-h}^{-h+h}\frac{\gamma R_* e^{\gamma Z}}{\rho c_p}\,dZ \qquad (10)$$

(Note that in (10) the vertical advection term has been included since this region is below the mixed layer and vertical temperature gradients do exist.) The integration above results in

$$\left(\frac{\partial T}{\partial t}+\mathbf{V}\cdot\nabla T\right)\Delta h+\left(T_S-T_{-h}\right)\left(w+\frac{\partial h}{\partial t}\right)+\overline{w'T'}\Big|_{-h+\Delta h}$$

$$=\frac{\gamma R_* \rho^{-\gamma h}\Delta h}{\rho_o c_p} \qquad (11)$$

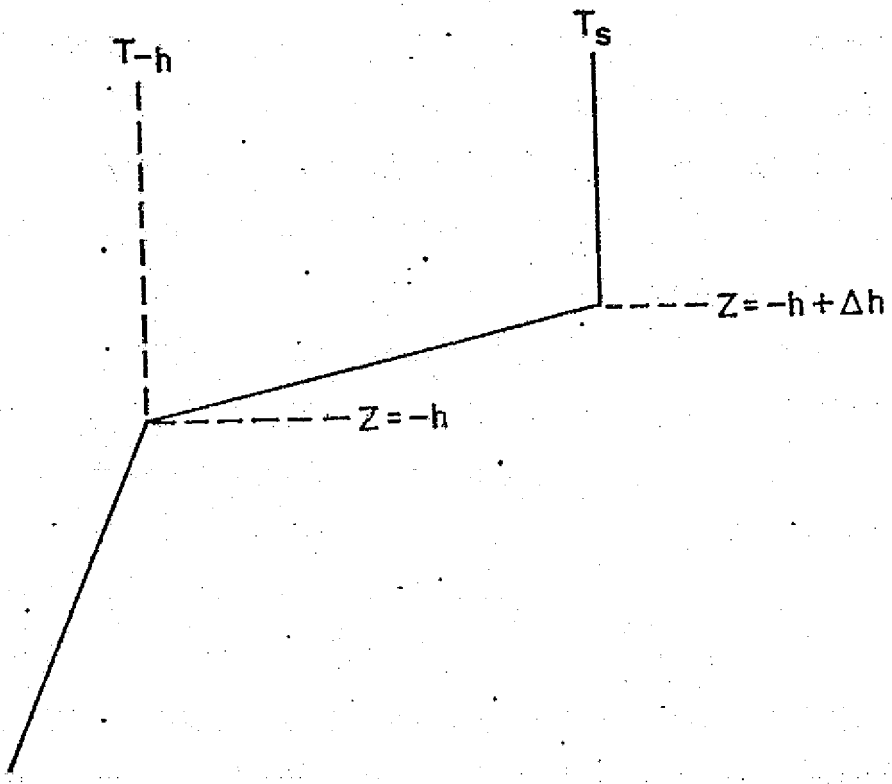

Fig. 3. Enlargement of the interface at the bottom of the mixed layer.

If we neglect horizontal variations in h and allow $\Delta h \to 0$ as depicted in Figures 2 and 3, then following Denman (1973),

$$\overline{w'T'}\Big|_{-h} = -H(w+\frac{dh}{dt})(T_s - T_{-h}) \tag{12}$$

where H is the Heaviside step function (defined previously).

At the top of the mixed layer, the turbulent heat flux is equal to the net heat transfer across the ocean surface. Thus,

$$\overline{wT}\Big|_o = -F \tag{13}$$

at the upper boundary, where

$$F = H_s + H_e + B. \tag{14}$$

Within the mixed layer itself, following Denman (1973), integration of the thermodynamic energy equation (7) with the aid of 12 and 13 results in

$$h(\frac{\partial T_s}{\partial t} + \bar{v}\cdot\nabla T_s + H(w+\frac{dh}{dt})(T_s - T_{-h}) = F + R(1-e^{-\gamma h}) \quad , \tag{15}$$

where $\bar{v}$ is the vertically integrated current in the mixed layer, i.e.

$$\bar{v} \equiv \frac{1}{h}\int_{-h}^{o} v\,dz \quad . \tag{16}$$

Integration of the steady state mechanical energy equation (9) within the mixed layer results in

$$-\int_{-h}^{o}\overline{s'w'}\frac{\partial S}{\partial z}dz - w'(\frac{p'}{\rho o}+\frac{c^2}{2})\Big|_{z=0}$$

$$= \alpha g\int_{-h}^{o}\overline{w'T'}\,dz + \int_{-h}^{o}\epsilon\,dz \tag{17}$$

where it has been assumed that

$$w'\left(\frac{p'}{\rho_0}+\frac{c^2}{2}\right)_{Z=-h} = 0 \quad .$$

From (17) it follows that

$$\int_{-h}^{0} \overline{w'T'}\, dZ = \frac{1}{\alpha g}\int_{-h}^{0} \overline{S'w'}\frac{\partial S}{\partial Z}dZ - \overline{w'\left(\frac{p'}{\rho_0}+\frac{c^2}{2}\right)}\Big|_{Z=0} - \frac{1}{\alpha g}\int_{-h}^{0}\varepsilon dZ \qquad (18)$$

If we let

$$G_* = -\rho_0 \int_{-h}^{0} \overline{S'w'}\,\frac{\partial S}{\partial Z}\,dZ - \rho_0 \overline{w'\left(\frac{p'}{0}+\frac{c^2}{2}\right)}\Big|_{Z=0}$$

$$D_* = \rho_0 \int_{-h}^{0} \varepsilon\, dZ \qquad (19)$$

and $G = -\frac{G_*}{\rho_0 \alpha g}$, $D = -\frac{D_*}{\rho_0 \alpha g}$

then

$$-\int_{-h}^{0} \overline{w'T'}\, dZ = G - D \qquad (20)$$

Following Denman (1973), if we now integrate equation 7 twice with respect to Z and combine it with equation 20 we arrive at

$$\frac{\partial T_s}{\partial t} + \bar{V}\cdot\nabla T = \frac{2}{h^2}[-(G-D) + Fh + R(h-\gamma^{-1}) + \gamma^{-1}Re^{-\gamma h} \qquad (21)$$

We can eliminate the terms on the left hand side of (21) by combining equations 15 and 21. This results in

$$H\left(w+\frac{dh}{dt}\right) = \frac{2[G-D+R\gamma^{-1}(1-e^{-\gamma h})]-h\,[F+R(1+e^{-\gamma h})]}{h(T_s-T_h)} \qquad (22)$$

for the region below $Z = -h$, while at $Z = -h$

$$\frac{d}{dt}(T-h) = \gamma R e^{-\gamma h} - (w + \frac{dh}{dt}) \frac{\partial T}{\partial Z}\Big|_{-h} \tag{24}$$

Here it has been assumed that no turbulent energy penetrates below $Z=-h$ and as mentioned earlier no currents exist at $Z = -h$ or below.

We can now restate the complete set of equations for the advective mixed-layer model as

$$\frac{\partial T_s}{\partial t} + \bar{V} \cdot \nabla T = \frac{2}{h^2}[-(G-D) + h(B+He+Hs) + R(h - \gamma^{-1} + \gamma^{-1} e^{-\gamma h})] \tag{25}$$

$$H[w + \frac{dh}{dt}] = \frac{2[G-D+R\gamma^{-1}(1-e^{-\gamma h})] - h(B+He+Hs+R(1+e^{-\gamma h}))}{h(T_s - T_h)} \tag{26}$$

$$\frac{d}{dt} T_{-h} = \gamma R e^{-\gamma h} - (w + \frac{dh}{dt}) \frac{\partial T}{\partial Z}\Big|_{-h} \tag{27}$$

As can be seen, this system of equations is almost identical to Denman's (equations 3-5 in this paper) and differs primarily in the inclusion of the horizontal advective term $\bar{V} \cdot \nabla T$ in equation 25 . All of the parameters for the above model are readily available from routine meteorological and oceanographic data with the exception of G and D. Denman assumes that we may approximate the term G - D as follows

$$G - D = \frac{mEa}{\rho_0 \alpha g} \tag{28}$$

In the above equation, m is a constant fraction of the rate of transfer of turbulent energy downward from the wind field

at 10 meters, and E_a the rate of work done by the wind stress at 10 meters is equal to $\rho_a C_{10} \bar{U}_{10}^3$, where ρ_a is the density of the air, C_{10} is the drag coefficient at 10 meters and $\bar{U}_{10}$ is the mean wind at 10 meters. Miller (1975) has found that this formulation results in too much deepening of the mixed layer during the cooling season and has empirically modified (28) so that for the cooling season only

$$G - D = \frac{mEa}{\rho_0 \alpha g} + .4\, h \frac{dA}{dt} \quad , \tag{29}$$

where

$$A = \int_{-h}^{0} T\, dZ \quad .$$

The addition of this empirical factor results in a more realistic prediction for the change in potential energy of the mixed layer and hence the deepening of this layer during the cooling season.

We may solve the system of equations (25 - 27) by first separating equation 25 into advective and non-advective parts. If we assume that there is horizontal homogeneity in the immediate vicinity of each gridpoint but that the entire ocean is not horizontally homogeneous, then as previously noted, we may utilize the modified Denman model (without the advective terms) to account for the SST changes due to solar and back radiation, air-sea heat exchange, and mixed-layer depth changes at each gridpoint. The advective temperature

change may then be computed independently at all gridpoints. The combination of these two calculations results in the final SST prediction for each gridpoint.

This process may be stated more precisely by the following steps:

1.) Solve equations 25-27 at each gridpoint with the term $\bar{V} \cdot \nabla T$ omitted. These one-dimensional calculations result in independent predictions for T_s, h, and T_{-h} at each gridpoint.

2.) Solve the advection scheme (to be discussed in the next subsection) for all gridpoints. This results in an additional heat flux term for the mixed layer.

3.) Add the predicted advective temperature change to the mixed layer calculation at each gridpoint and adjust the final prediction of T_s, h, and T_{-h} to account for the addition or removal of heat from the mixed layer due to horizontal advection.

3.3 The Advection Scheme

The advection scheme to be described herein consists of (1) specifying an ocean current field for the entire horizontal grid, (2) solving the advective parts of the equations for conservation of heat and mass for the entire

horizontal grid, and (3) determining the change in temperature at each gridpoint due to the net heat and mass transfers at these points.

In Section 1, it was stated that the advection scheme must include the effects of both mean ocean currents and anomalous wind-generated currents, in order to carry out the objectives of this study. As a generalization of the approach used by Adem (1970) we assume that,

$$\mathbb{V} = \mathbb{V}_M + (\mathbb{V}_{AD} - \mathbb{V}_{MD}) + \mathbb{V}_G \quad . \tag{30}$$

In the above equation the total ocean current $\mathbb{V}$ has been divided into its mean and anomalous parts, where $\mathbb{V}_M$ is the mean monthly or seasonal ocean current (specified from climatology, $\mathbb{V}_{AD}$ is the drift current computed from the actual (observed or predicted wind), $\mathbb{V}_{MD}$ is the drift current computed from the mean monthly or seasonal winds, and $\mathbb{V}_G$ is an anomalous geostrophic current, computed from anomalous changes in the sea surface slope. From the definition of the vertically averaged current in the mixed layer (equation 16) we may define

$$\begin{aligned} \bar{\mathbb{V}}_M &= \frac{1}{h} \int_{-h}^{0} \mathbb{V}_M \, dZ \\ \bar{\mathbb{V}}_{MD} &= \frac{1}{h} \int_{-h}^{0} \mathbb{V}_{MD} \, dZ \\ \bar{\mathbb{V}}_{AD} &= \frac{1}{h} \int_{-h}^{0} \mathbb{V}_{AD} \, dZ \\ \bar{\mathbb{V}}_g &= \mathbb{V}_g \end{aligned} \tag{31}$$

and $$\bar{V} = \bar{V}_M + (\bar{V}_{AD} - \bar{V}_{MD}) + V_G \qquad (32)$$

Thus the total current through the mixed layer consists of both mean and anomalous components. The fields of $\bar{V}_M$ which were used in this study were prepared by the author and are described in the next section. As mentioned, this field is specified and does not change with time. $\bar{V}_{MD}$ represents the pure wind driven part of $\bar{V}_M$ and also does not change with time. $\bar{V}_{AD}$ on the other hand, represents the pure wind driven current due to varying atmospheric winds and therefore at any instant of time ($\bar{V}_{AD} - \bar{V}_{MD}$) represents the anomalous wind driven ocean current.

Both of these drift currents are computed from Ekman theory. According to this theory (Adem 1970 or Neumann 1968), whenever a wind blows over the ocean surface, pure wind drift currents are generated by the transfer of momentum from the wind stress to the water and by the friction between moving layers of water. Surface drift currents in the Northern Hemisphere are directed 45° to the right of the wind direction while each succeedingly lower layer is directly at an increasing greater angle and slower speed than the layer immediately above it. The level at which the current speed has decreased to $e^{-\pi}$ of its surface value and its direction is exactly opposite to the surface current direction

is referred to as the depth of friction influence. Within the layer of frictional influence, above the depth, the total current transport vector is directed 90° to the right of the wind and its magnitude is equal to 0.225 times the magnitude of the surface current. These principles may be expressed by the following formulas:

$$V_{DX} = V_0 \, e^{-(\pi/D)Z} \cos\left(\frac{\pi}{4} - \frac{\pi}{D}Z\right)$$
$$V_{DY} + V_0 \, e^{-(\pi/D)Z} \sin\left(\frac{\pi}{4} - \frac{\pi}{D}Z\right) \qquad (33)$$

where V_{DX} is the component of the pure drift current at a depth Z, which is perpendicular to the surface wind direction, V_{DY} is the component of the pure drift current at a depth Z, which is parallel to the surface wind direction, V_o is the speed of the surface current, and D is the depth of frictional influence. At the surface $Z = 0$ and

$$V_{DX} = V_0 \cos\frac{\pi}{4}$$
$$V_{DY} = V_0 \sin\frac{\pi}{4} \qquad (34)$$

while at the depth of frictional influence $Z = D$ and

$$V_{DX} = V_0 e^{-\pi} \cos\left(\frac{\pi}{4} - \pi\right)$$
$$V_{DY} = V_0 e^{-\pi} \sin\left(\frac{\pi}{4} - \pi\right) \qquad (35)$$

Empirical values for the surface current speed V_0 and the depth of frictional influence D have been determined by Thorade (see Adem 1970). For surface wind speeds greater than 6 meters per second,

$$V_0 = \frac{0.0127}{\sqrt{\sin \phi}} W \tag{36}$$

(which is the same as equation 1)

and $$D = \frac{7.6\ W}{\sqrt{\sin \phi}}$$

For winds speeds less than or equal to 6 meters per second

$$V_0 = \frac{0.0259}{\sqrt{\sin \phi}} \sqrt{W} \tag{37}$$

and $$D = \frac{3.67\ \sqrt{W}}{\sqrt{\sin \phi}}$$

From the above formulas we may now state our equations for evaluating the pure mean or actual wind drift velocity components through a depth h (equal to the mixed-layer depth) as

$$\bar{u}_D = C \frac{0.0127}{\sqrt{\sin \phi}} (u_W \cos \theta + v_W \sin \theta) \quad \text{for} \quad W > 6 \text{ m sec}^{-1}$$

$$\bar{v}_D = C \frac{0.0127}{\sqrt{\sin \phi}} (v_W \cos \theta - u_W \sin \theta) \quad \text{for} \quad W > 6 \text{ m sec}^{-1} \tag{38}$$

or

$$\bar{u}_D = C \frac{0.0259}{\sqrt{\sin \phi}} (u_W \cos \theta + u_W \sin \theta) \quad \text{for} \quad W \leq 6 \text{ m sec}^{-1}$$

$$\bar{v}_D = C \frac{0.0259}{\sqrt{\sin \phi}} (v_W \cos \theta - u_W \sin \theta) \quad \text{for} \quad W \leq 6 \text{ m sec}^{-1} \tag{39}$$

where $\bar{u}_d$ and $\bar{v}_d$ are the west-east and south-north components of the mean or actual drift current through the mixed layer, u_w and v_w are the mean or actual wind components in the west-east and south-north directions, θ is the angle between the wind and the total wind driven current through the mixed-layer, and C is a current magnitude factor. In order to determine the parameters C and θ, it is necessary to compute the depth of frictional influence D from equations 36 or 37 and compare this value to the mixed-layer depth h. If h is greater than or equal to D then we assume following Ekman that the drift current speeds below the depth D are negligibly small and we set $C = 0.225$ and $\theta = 90^{\circ}$. If h is less than D then C will lie between 1 and 0.225 and θ will be between 45° and 90°. The exact value for C and θ depends on the ratio h/D.

Namias, (1959) Eber, (1961) and Jacob (1967) used values for C and θ of 1 and 45° respectively while Clark (1972) and Adem (1970) tested their model with values of 0.225 and 90° as well. They found that their best results were obtained with values of $C = 1$ and $\theta = 45^{\circ}$. However the author feels that it is not reasonable to consider the surface current (as indicated by these values for C and θ) to extend throughout the entire mixed-layer depth. The approach taken here has been to allow convergence or diver-

gence of anomalous drift currents to result in changes in the height of the sea surface at each primary gridpoint. From the sea surface slope so created, we may compute the anomalous geostrophic current V_g. The components of this geostrophic current u_g and v_g are given by the following formulas:

$$u_g = \frac{-g}{2\Omega \sin\phi} \frac{\Delta Z}{\Delta Y}$$

$$v_g = \frac{g}{2\Omega \sin\phi} \frac{\Delta Z}{\Delta X} \qquad (40)$$

where ΔZ is the change in the height of the sea surface, $\frac{\Delta Z}{\Delta Y}$ and $\frac{\Delta Z}{\Delta X}$ represent the anomalous sea surface slope, and Ω is the earth's angular velocity. The combination of the geostrophic and wind driven components results in a total current through the mixed layer, which has a larger magnitude and smaller angle of deviation from the wind than the original drift current. This approach is consistent with Ekman's "elementary current system" (see Neumann 1968) and provides a somewhat sounder theoretical basis for the advection scheme.

The grid system used in this model is a simplified version of the "box method" (Kurihara 1967) and has the property of conserving both heat and mass for the advective calculation. Specifically the grid consists of a series of

grid boxes, at the center of which are the primary grid-points of the GISS model (described earlier). A section of this grid is depicted in Figure 4. Each individual grid box is horizontally homogeneous in all properties. However, the entire ocean is not assumed to be homogeneous. As previously mentioned, this approach enables us to apply the modified Denman model at each of the primary gridpoints depicted by dots in Figure 4 to predict T_s, h, and T_{-h} non-advectively. The ocean current values are computed at each of the secondary gridpoints depicted by circles in Figure 4. Averaging of these current values at the four corners of each box results in the net zonal and meridional currents for that box. This in turn is used to account for the net heat and mass transfer through each box. In this manner, heat and mass are exchanged between neighboring grid boxes and the temperature advection calculation for the entire grid is accomplished.

If we consider each primary gridpoint to be specified by the index i,j (where the i value represents the longitude, and the j value represents the latitude), then we may specify the four secondary gridpoints surrounding the primary gridpoint as $(i+\frac{1}{2}, j+\frac{1}{2})$, $(i+\frac{1}{2}, j-\frac{1}{2})$, $(i-\frac{1}{2}, j-\frac{1}{2})$ and $(i-\frac{1}{2}, j+\frac{1}{2})$, and the four sides of the gridbox as $(i+\frac{1}{2}, j)$, $(i, j-\frac{1}{2})$, $(i-\frac{1}{2}, j)$ and $(i, j+\frac{1}{2})$. This specification is depicted in Figure 5. The mass transport across each grid box side can be computed from the following quantities:

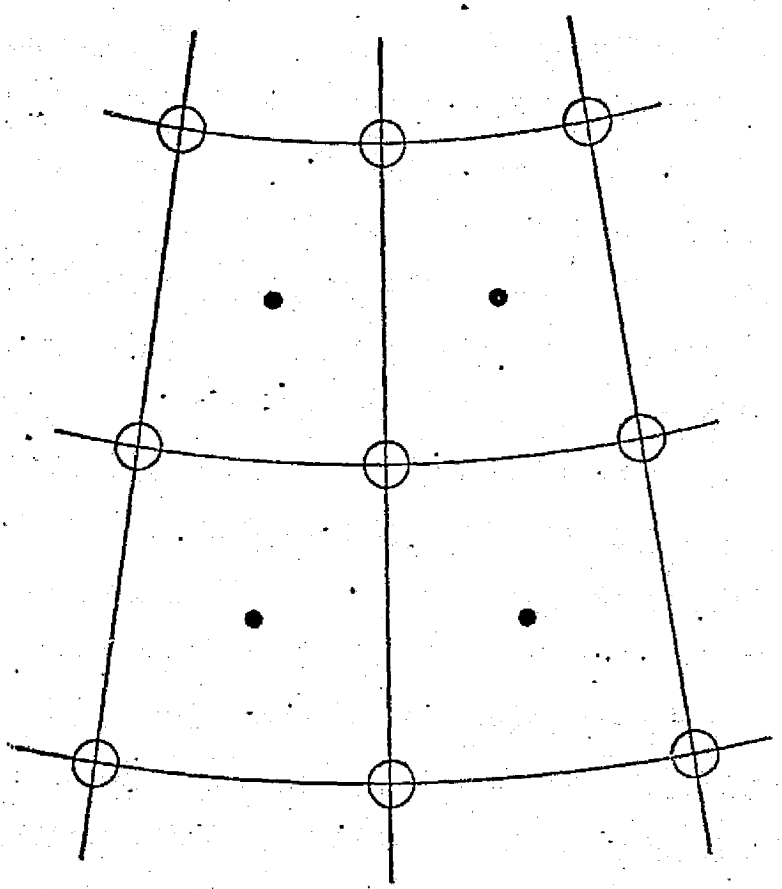

Fig. 4. A section of the grid for the advective canculation. Dots represent primary gridpoints. Circles represent secondary gridpoints.

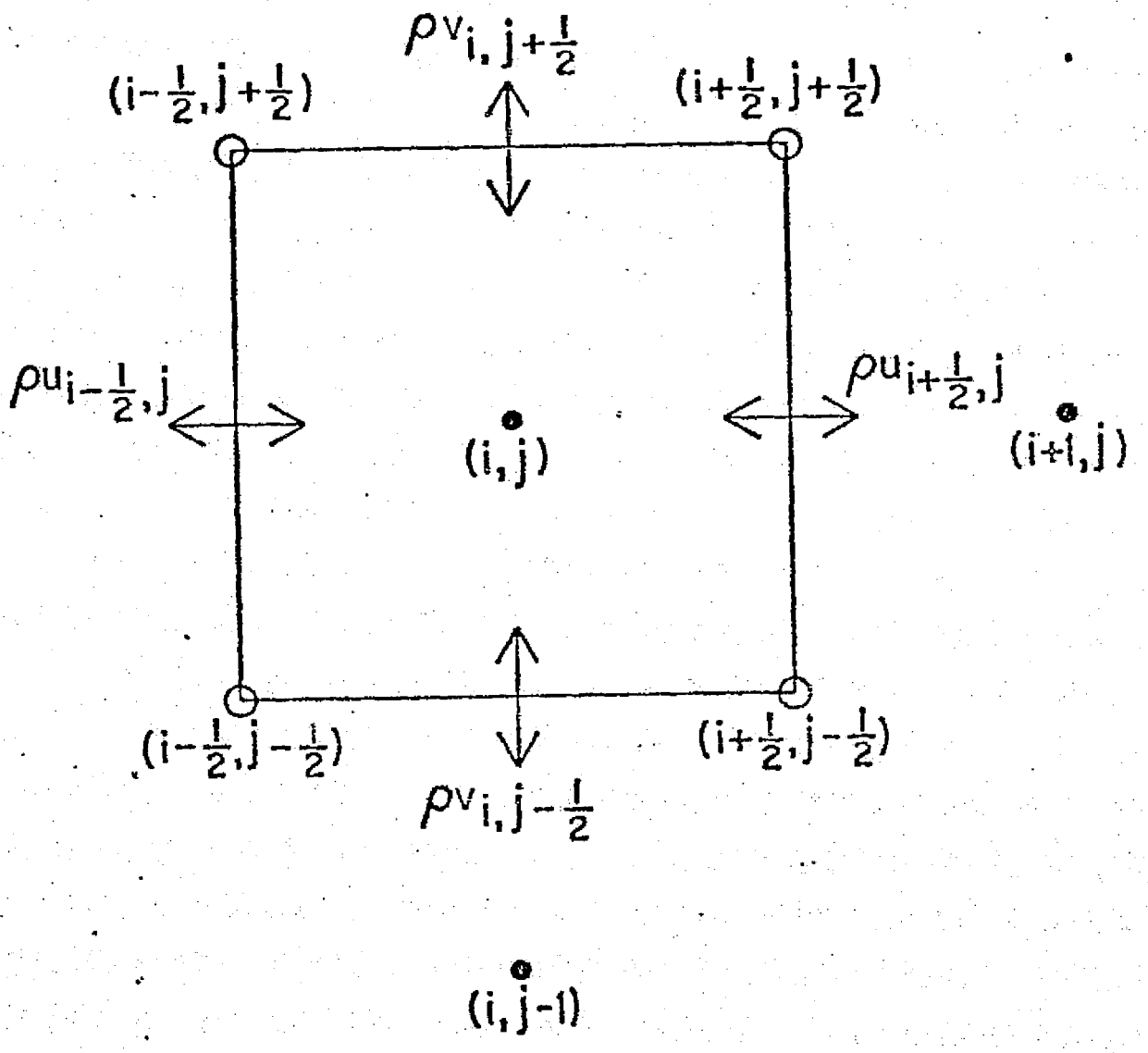

Fig. 5. Schematic diagram of box method computation.

$$\frac{\rho}{2}(u_{i+\frac{1}{2},j+\frac{1}{2}} + u_{i+\frac{1}{2},j-\frac{1}{2}})\ \Delta Y_j \text{ h mean}$$

$$\frac{\rho}{2}(u_{i-\frac{1}{2},j+\frac{1}{2}} + u_{i-\frac{1}{2},j-\frac{1}{2}})\ \Delta Y_j \text{ h mean} \qquad (41)$$

$$\frac{\rho}{2}(v_{i-\frac{1}{2},j+\frac{1}{2}} + v_{i+\frac{1}{2},j+\frac{1}{2}})\ \Delta X_i \text{ h mean}$$

$$\frac{\rho}{2}(v_{i-\frac{1}{2},j-\frac{1}{2}} + v_{i+\frac{1}{2},j-\frac{1}{2}})\ \Delta X_i \text{ h mean}$$

where ΔY_j is the distance between secondary j gridpoints (equal to 4° of latitude), ΔX_i is the distance between secondary i gridpoints (equal to 5° of longitude), and h mean is the mean depth of the ocean current across that side of the grid box. Summing up these four transports results in the net mass transport into the box. If there is net mass convergence into the box, then ΔZ (the change of the sea surface height at the primary gridpoint) will be positive and the sea surface will rise. If there is a net divergence for the box, then ΔZ will be negative and the sea surface will fall. From the new values for Z at each primary gridpoint, the anomalous geostrophic current V_g can be computed from equations 40. These equations can be restated in finite difference form as

$$u_g = \frac{g}{2\,\Omega \sin\,\phi}\,\frac{(Z_{i,j-1} - Z_{i,j+1})}{2\Delta Y_j}$$

$$v_g = \frac{g}{2\,\Omega \sin\,\phi}\,\frac{(Z_{i+1,j} - Z_{i-1,j})}{2\Delta Y_i} \qquad (42)$$

The thermodynamic energy equation for the advective part of the calculation is

$$\frac{\partial T_s}{\partial t} = -u\frac{\partial T_s}{\partial x} - v\frac{\partial T_s}{\partial y} \tag{43}$$

where u and v are the west-east and south-north components of the total current in the mixed layer. Multiplication of this equation by the density ρ and combination with the continuity equation results in the flux form of the advective equation,

$$\frac{\partial}{\partial t}(\rho T_s) = -\frac{\partial}{\partial x}(\rho u T_s) - \frac{\partial}{\partial y}(\rho v T_s). \tag{44}$$

In order to compute the heat fluxes into the box, we must consider the difference in temperature between the water inside the box and the water surrounding the box. The heat fluxes across each side of the box may be computed from

$$\begin{aligned}
(\rho\bar{u}T_s)_{i+\frac{1}{2},j} &= \rho\bar{u}_{i+\frac{1}{2},j}\left(\frac{T_{s_{i,j}} + T_{s_{i+1,j}}}{2}\right) \\
(\rho\bar{u}T_s)_{i-\frac{1}{2},j} &= \rho\bar{u}_{i-\frac{1}{2},j}\left(\frac{T_{s_{i,j}} + T_{s_{i-1,j}}}{2}\right) \\
(\rho\bar{v}T_s)_{i,j+\frac{1}{2}} &= \rho\bar{v}_{i,j+\frac{1}{2}}\left(\frac{T_{s_{i,j}} + T_{s_{i,j+1}}}{2}\right) \\
(\rho\bar{v}T_s)_{i,j-\frac{1}{2}} &= \bar{v}_{i,j-\frac{1}{2}}\left(\frac{T_{s_{i,j}} + T_{s_{i,j-1}}}{2}\right)
\end{aligned} \tag{45}$$

The local temperature tendency within the box is then calculated from the divergence of the heat flux, and the temperature at each gridpoint is predicted by the Euler method. Stated simply, the predicted temperature at the primary gridpoint is equal to the original heat content of the box plus the heat flux into the box, divided by the new volume of the box.

4. Climatological Simulation with the Advective Mixed-Layer Model

The initial phase of experimentation with the advective mixed-layer model was designed to (1) test the model's ability to predict climatological SST variations, (2) determine if the inclusion of advection results in an improvement in the predictive skill of the mixed-layer model, and (3) determine the relative importance of advection and mixed-layer depth changes. Two 3-month prediction experiments, one in the cooling season and one in the heating season, were conducted. We shall refer to these as experiments 1 and 2 respectively.

Data for these two experiments consisted of (1) initial conditions of the monthly mean SST and mixed-layer profiles for each of the primary gridpoints, (2) climatological values for the solar and back radiation, wind speed, and sensible and latent heat fluxes, at each primary gridpoint, (3) climatological ocean current values in component form at each of the secondary gridpoints, and (4) monthly mean SST fields for verification. All of the SST data for these two experiments were derived from the monthly mean ocean temperature tabulation developed at the National Center for Atmospheric Research (Washington and Thiel 1970). The

climatological mixed-layer profiles were derived from the Mechanical Bathythermograph (MBT) Data File of the National Oceanographic Data Center. This data file consists of vertical profiles of temperature, with observations at five meter intervals. The mixed-layer depth was taken to be the first point on the profile where the decrease of temperature with depth is $.2^{o}C/5$ meters or more.

The mean fluxes were taken directly from a tabulation of such data by Schutz and Gates (1971). The data used by the author to prepare the mean ocean current field consisted of (1) climatological observations of surface ocean currents, obtained from the Climatological and Oceanographic Atlas for Mariners, Volumes 1 and 2 (1959, 1966). (2) a limited number of observations of the vertical variation of horizontal ocean currents, obtained from the Woods Hole Oceanographic Institution and from several standard oceanographic texts (Sverdrup et. al. 1942, Defant 1961, Stommel 1965, Neumann and Pierson 1966, Stommel and Yoshida 1972) and (3) a limited number of observations of the mean density fields for the Atlantic and Pacific oceans, also obtained from the Woods Hole Oceanographic Institution and the same standard oceanographic texts mentioned above. These sources of data enabled the author to make a subjective approximation to the vertical profiles of the horizontal ocean

current at each gridpoint and hence the average horizontal current in the mixed layer. Specifically the method followed was to (1) interpolate the surface ocean current values to the primary gridpoints of the advective model, (2) estimate the vertical variation of these currents with depth from the Ekman spiral theory, as described in the previous section, (3) modify the profiles so obtained using the limited number of vertical profile observations and estimates of the geostrophic current shear obtained from the density fields, (4) average the vertical profiles to obtain the mean current in the mixed layer, (5) divide these currents into their west-east and south-north components, and (6) interpolate these values to the secondary gridpoints.

In experiment 1, the prediction was made from January mean initial conditions and mean fluxes were updated daily to drive the model. The mean ocean current values for the three month period were specified and remained constant. Obviously the anomalous current terms ($\mathbf{V}_{AD} - \mathbf{V}_{MD}$) and $\mathbf{V}_g$ were equal to zero since the actual and mean winds were the same in these experiments. SST predictions from three different versions of the mixed-layer model were evaluated at the end of thirty, sixty, and ninety days. Version (A) refers to the original version of the GISS ocean model in which no advection is included. Version (B) is the same

as (A) except that in this case advection by mean ocean currents is included. Version (C) is the same as (B) except that in this case the mixed-layer depth is held constant with time and therefore no deepening is allowed to occur. This last case was included to illustrate the importance of mixed-layer deepening in the advective model, since earlier advective models of the upper ocean (Jacob 1967, Adem 1970, and Clark 1972) did not account for such mixed-layer depth changes. A fourth version, which we shall refer to as Version (P), represents the persistence forecast and is included for comparison, to determine if any of the three forecasts possess skill over persistence.

SST predictions were made for the entire Northern Hemisphere (between 2^{o}N and 70^{o}N) with the exception of the Indian Ocean. The results of this experiment and the one to follow were analyzed in terms of the absolute difference between the predicted and observed sea-surface temperature at each of the primary gridpoints, for the four different versions. These absolute errors were then added for the entire North Atlantic and North Pacific (between 2^{o}N and 70^{o}N) and then divided by the total number of gridpoints for each of these regions to yield the average absolute error for the North Atlantic and North Pacific. The average absolute temperature error for the four versions of the model is presen-

ted in Figures 6 and 7 for the North Atlantic and North Pacific respectively. From these figures, it can be seen that the advective effect, as represented by the difference between the A and B curves, is relatively large for both oceans and that the inclusion of advection has resulted in approximately a 50% reduction in the average absolute error of the SST predictions. The effect of mixed-layer depth changes, as represented by the difference between C and B is also large. In the North Atlantic, neglect of mixed layer variations (curve C) produces a forecast which is no better than that resulting from neglect of advection (curve A). For the North Pacific, inclusion of advection and neglect of mixed-layer depth variations (C) produces a forecast only slightly better than that of the non-advective GISS model (A). Clearly, both advection and mixed-layer depth variations must be included in the ocean mixed-layer model. In order to determine the skill of the A, B and C predictions over persistence, the average absolute error for these three model versions was compared with average absolute error of the P forecasts. It is clear from these figures, that although all three versions possess skill over persistence at thirty days, only the version B, which includes both advection and mixed-layer depth changes, consistently maintains predictive skill over persistence out to ninety days.

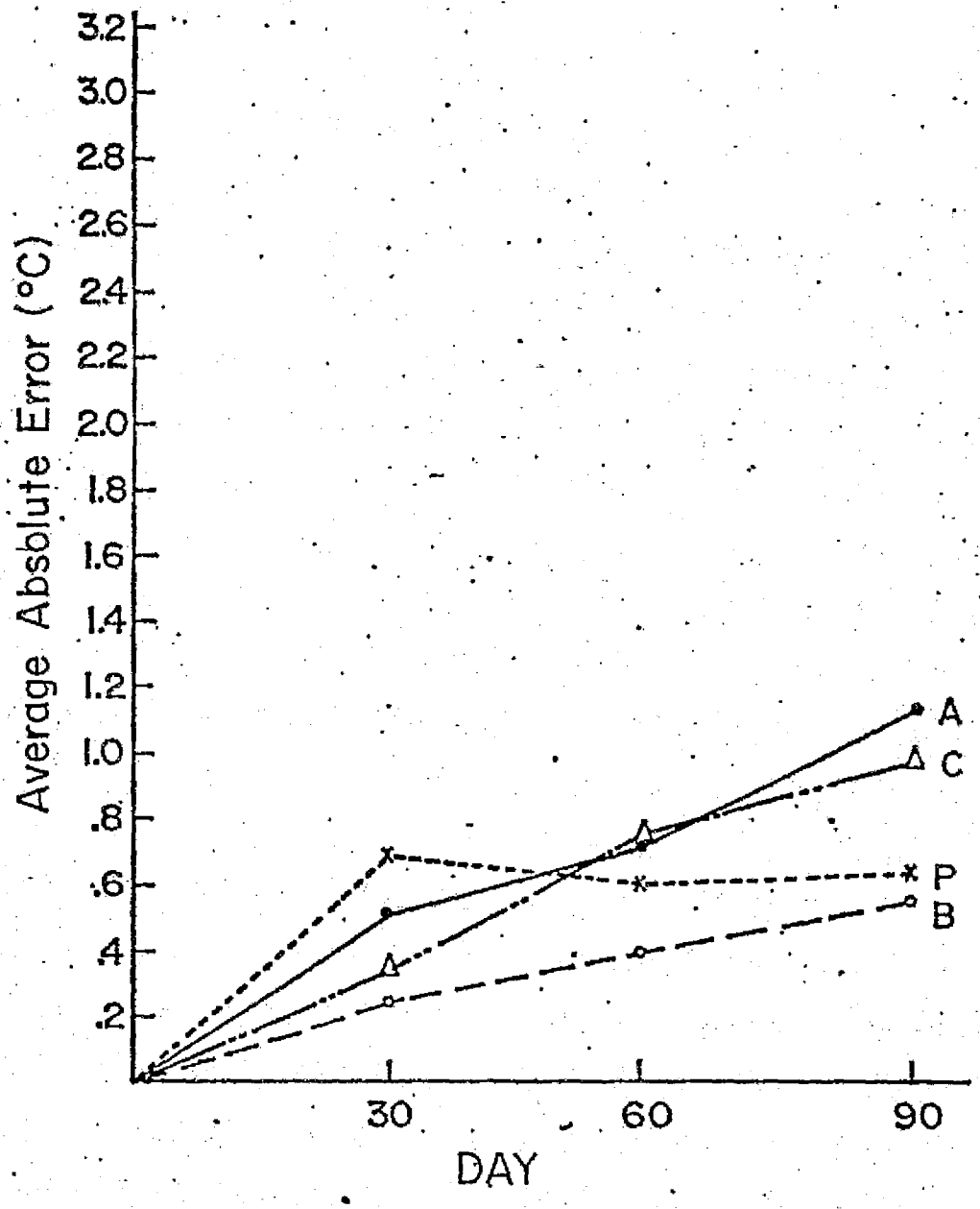

Fig. 6. Average absolute errors in predicted sea-surface temperatures (°C) over the North Atlantic, generated by versions (A), (B), (C) and (P) for the cooling season (January initial conditions).

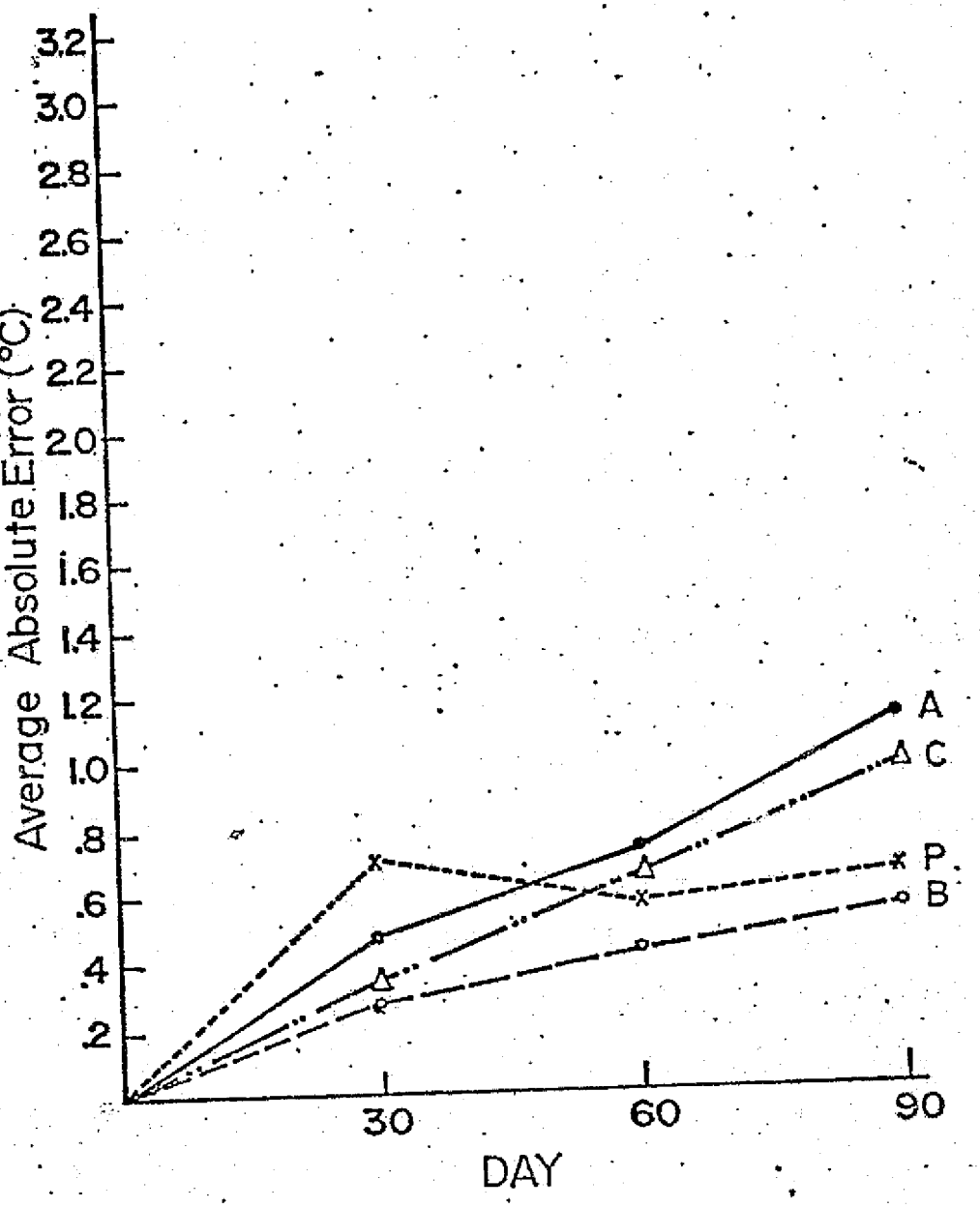

Fig. 7. Same as Fig. 6 for the North Pacific.

The significance of the advective effect is also illustrated by Figures 8 and 9. Figure 8 presents the error field for version A at the end of ninety days while Figure 9 presents the error field for version B at the end of ninety days. A comparison of the figures indicates that virtually all of the large errors have been eliminated as a result of the advective effect and only a few smaller errors remain. Some of these remaining errors are due to errors in the mean ocean current field while others may be due to the simplifying assumptions of the mixed layer model. A comparison of the absolute errors at each gridpoint for model versions A and B shows that for the North Atlantic, the predictions were improved at 71% of the gridpoints, remained the same at 10% and were worsened at 19% of the gridpoints by the inclusion of advection. For the North Pacific, the inclusion of advection resulted in an improvement of the predictions at 65% of the gridpoints, while 22% were worsened, and 13% remained unchanged. Clearly, errors in the mean current field are responsible for many of these advective errors. However, improvement of the field will probably not occur until sufficient observations of the vertical profiles of horizontal ocean currents are obtained. From Figures 8 and 9 it can be seen that the largest advective effects are associated with the major currents particularly the Gulf Stream,

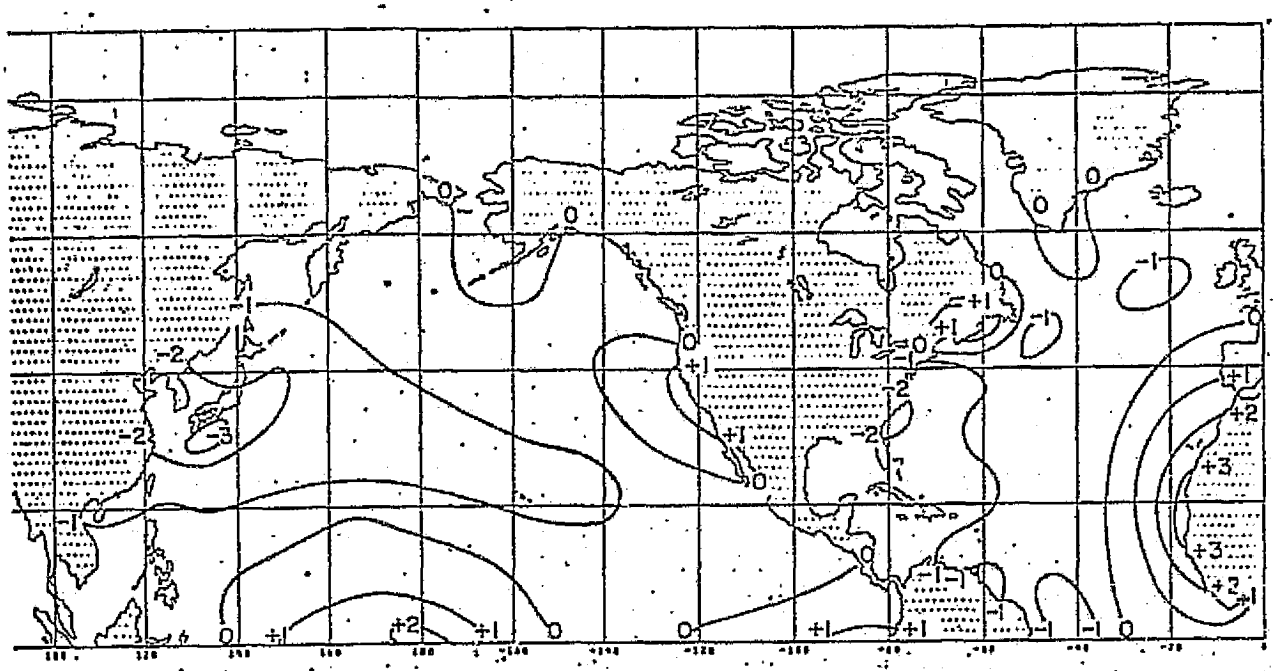

Fig. 8. Error field for the 90-day sea-surface temperature predictions from January mean initial conditions, using model version A. Solid lines are error isotherms drawn for an interval of 1°C.

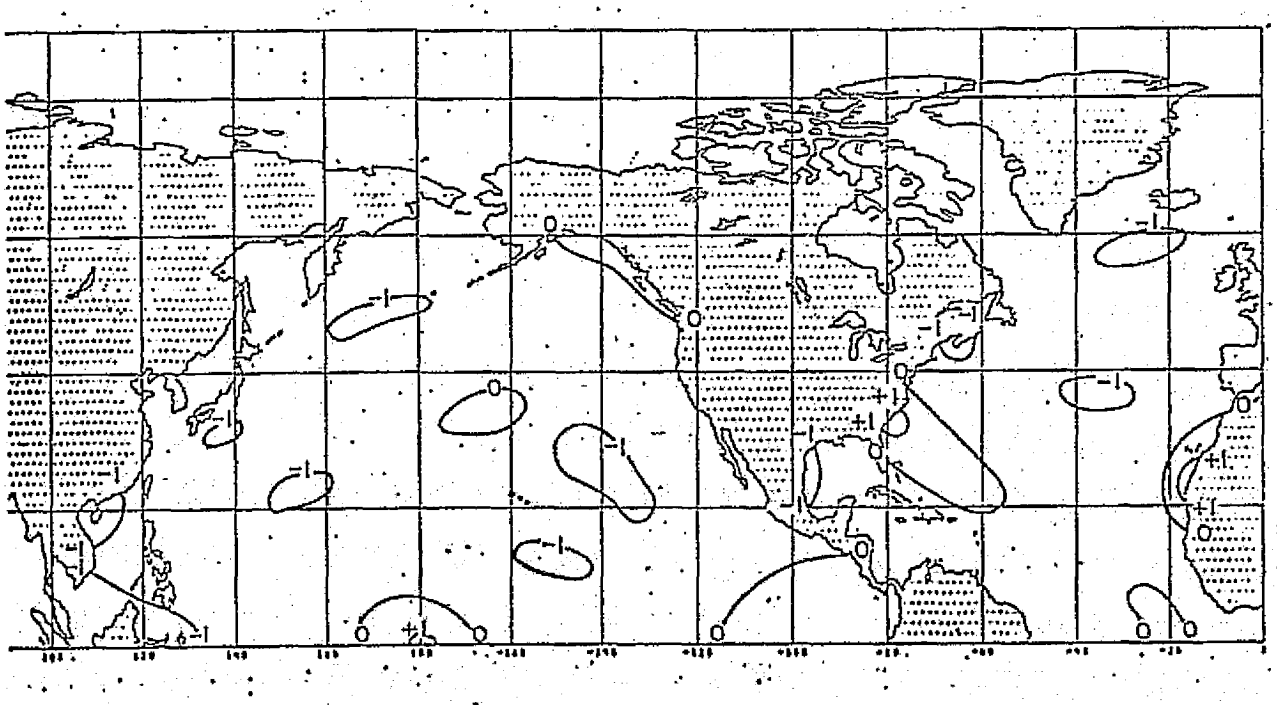

Fig. 9. Same as Fig. 8 for model version B.

Kuroshio, Labrador, Canary and California currents. Not enough advection of heat has occurred off the west coast of Africa or the southern tip of Japan, while too much advection has occurred along the east coast of the United States.

In order to gain further insight into the regional importance of the advective effect, the average absolute errors have been computed for the regions of the North Atlantic and North Pacific between 34°N and 70°N and between 2°N and 30°N. The graphs for the regions are presented in Figures 10-13. A comparison of Figures 10 and 11 reveals that the variability of the climatological SST field, as represented by the P curve, is considerably larger for the northern region of the North Atlantic than for the southern region, while the accuracy of the version B predictions are similar for both regions. This means that version B possesses somewhat more skill in the northern region than in the southern region and that the model is capable of predicting both large and small temperature changes. The advective effect and the effect due to mixed-layer depth changes are about equally large for both regions. However this latter effect is actually slightly larger and more important than the advective effect at sixty and ninety days for the northern region. A comparison of Figures 12 and 13 reveals similar

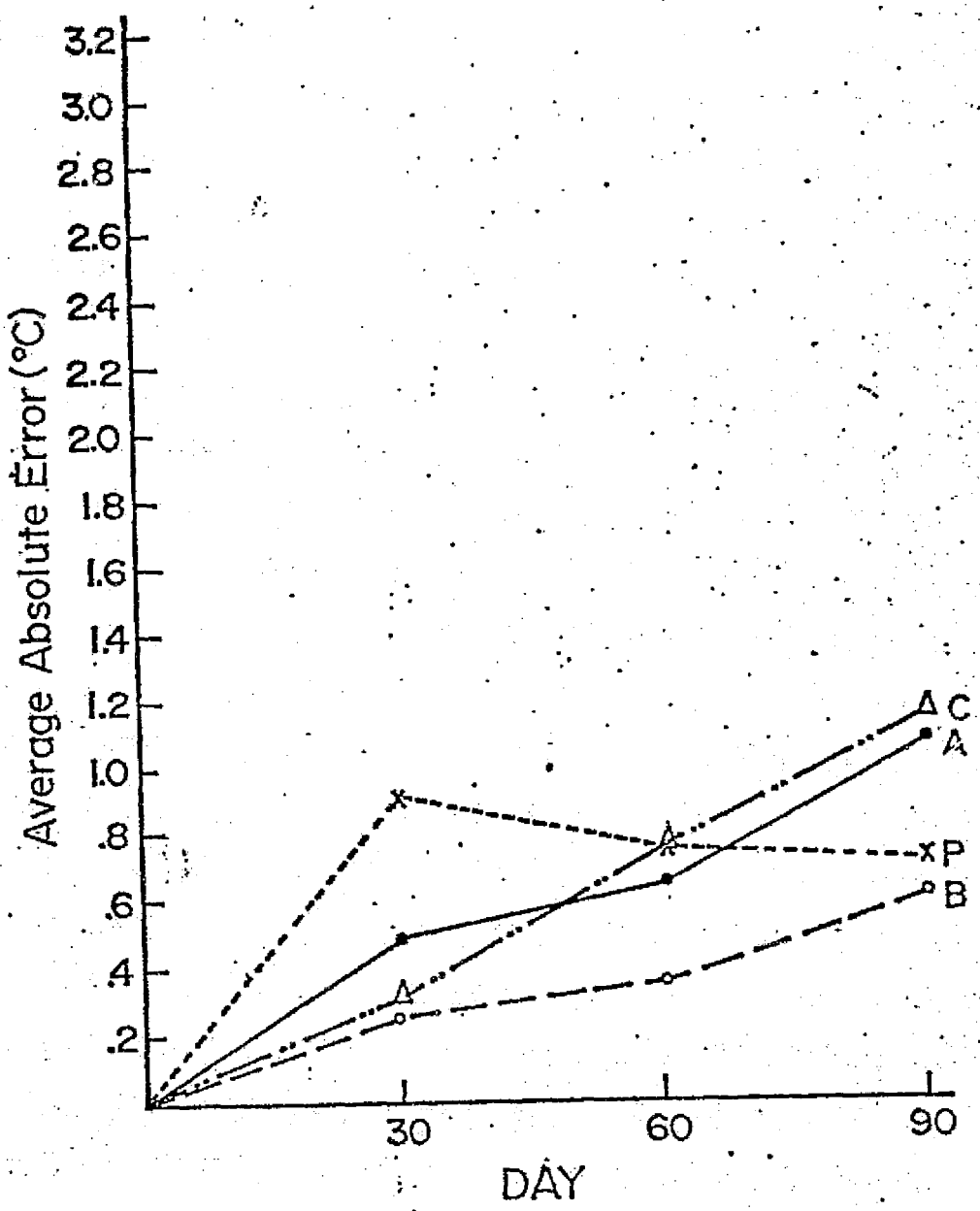

Fig. 10. Same as Fig. 6 for the North Atlantic between 34°N and 70°N.

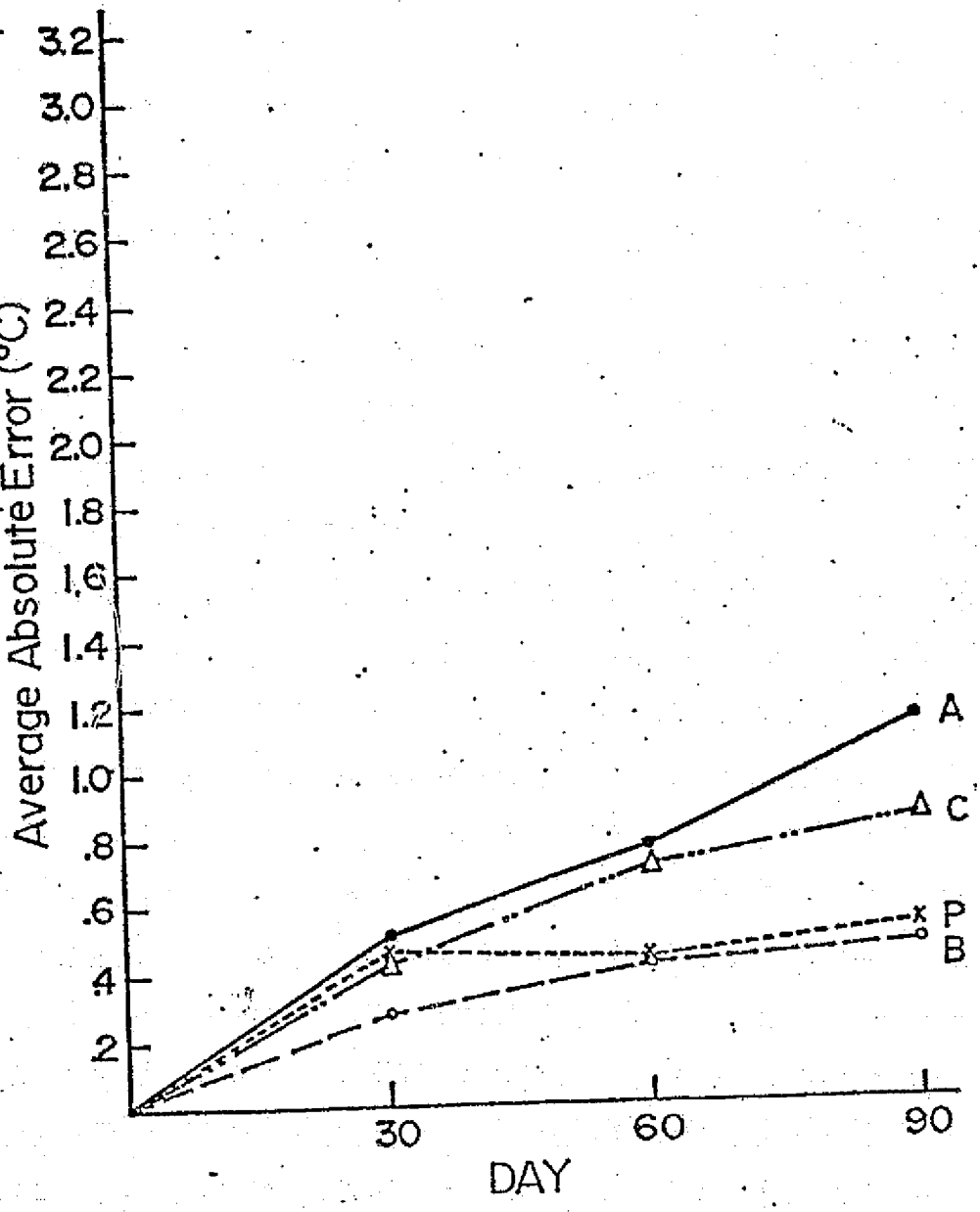

Fig. 11. Same as Fig. 6 for the North Atlantic between 20°N and 30°N.

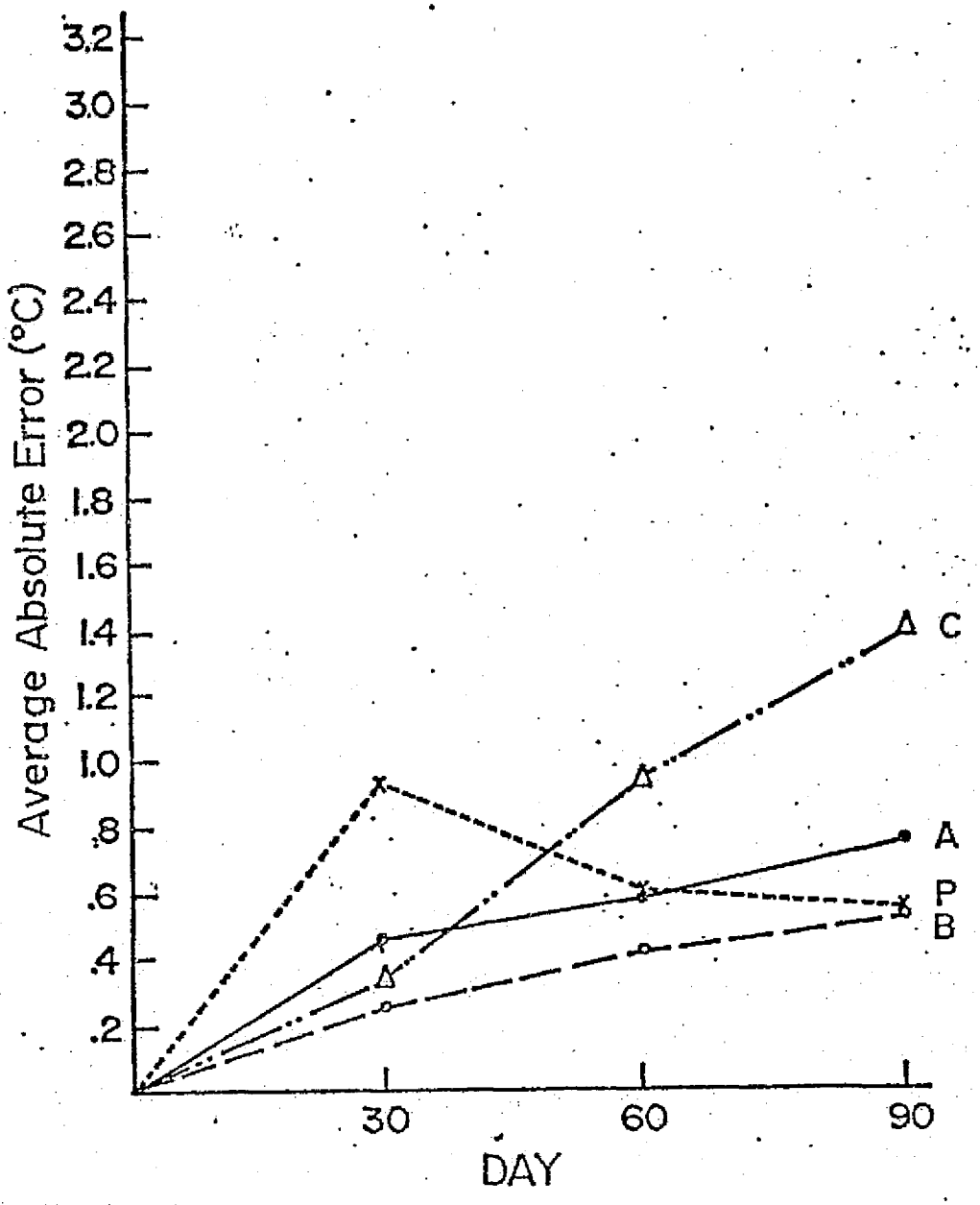

Fig. 12. Same as Fig. 6 for the North Pacific between 34°N and 70°N.

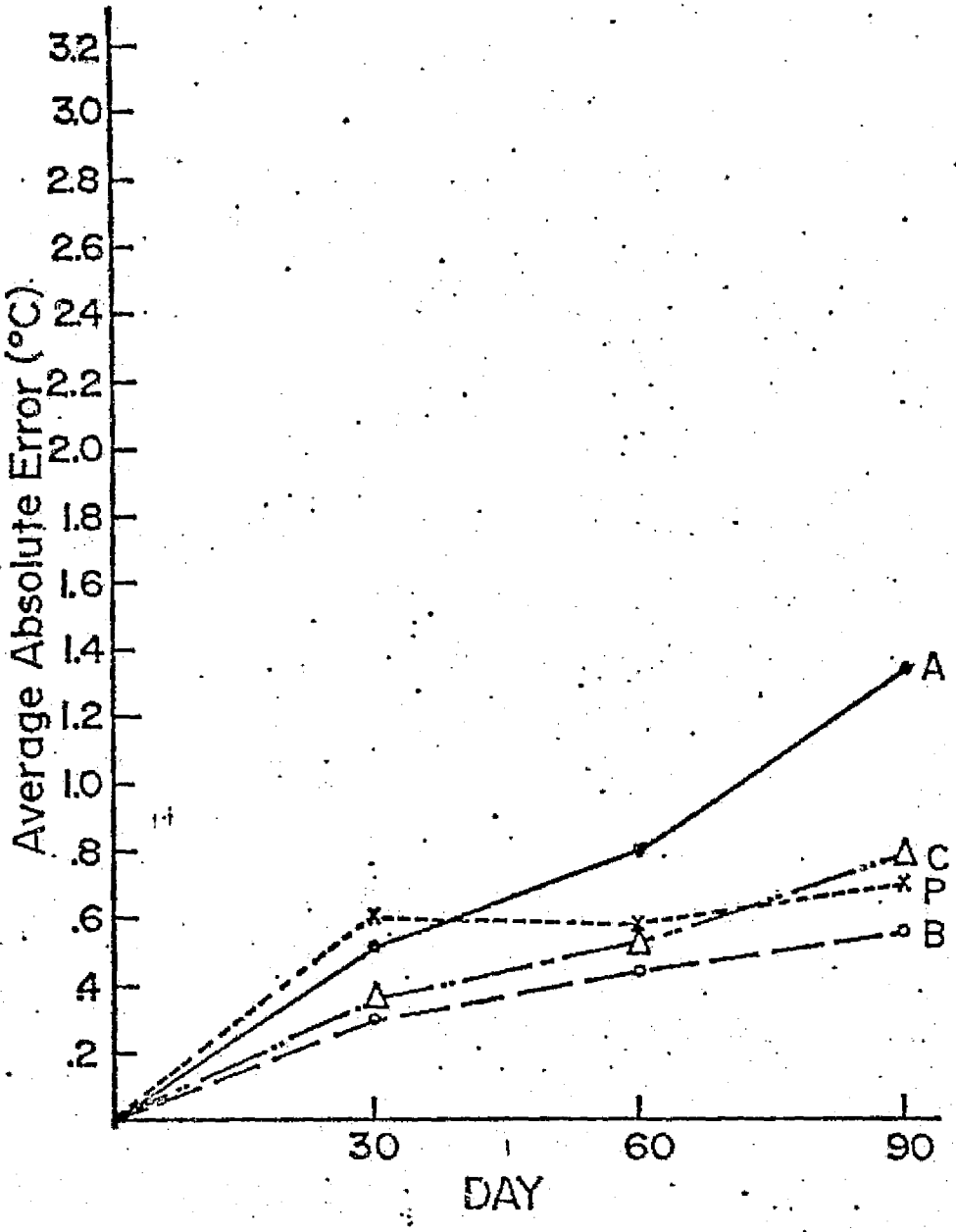

Fig. 13. Same as Fig. 6 for the North Pacific between 2°N and 30°N.

results. However, the effect due to mixed-layer depth changes is considerably larger than the advective effect for the northern regions of the North Pacific at sixty and ninety days.

In experiment 2, the ninety-day predictions were made from June initial conditions and the mean fluxes were again updated daily to drive the model. Data for this experiment was prepared from the same sources and in the same manner as in experiment 1. The summer mean current field differs from the winter mean current field primarily in the fact that the currents are considerably more meridional in direction in the North Pacific while being only slightly weaker in strength. Also the mixed-layer depths are much shallower in the summer experiment and therefore the upper level currents, when averaged over the entire mixed layer, are stronger.

The average absolute errors for versions A, B, C and P are presented in Figures 14 and 15 for the North Atlantic and North Pacific respectively. A comparison of these figures with Figures 6 and 7 shows that in experiment 2 the average absolute errors for version P is more than twice as large as in experiment 1 at thirty days and more than three times as large at sixty and ninety days. The average absolute error for versions A, B and C is only slightly larger in experiment 2. As a result of this, all three of these

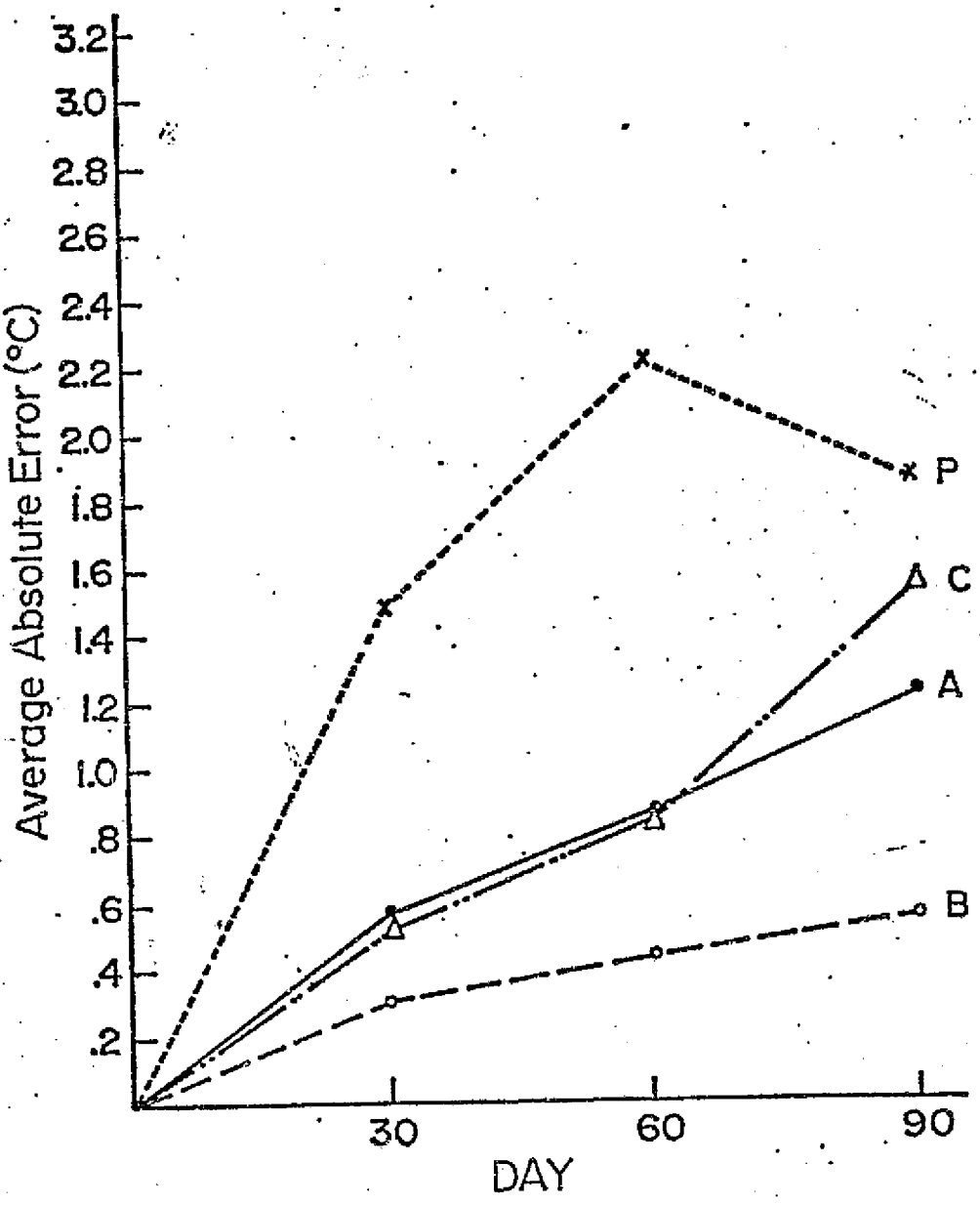

Fig. 14. Same as Fig. 6 for June initial conditions.

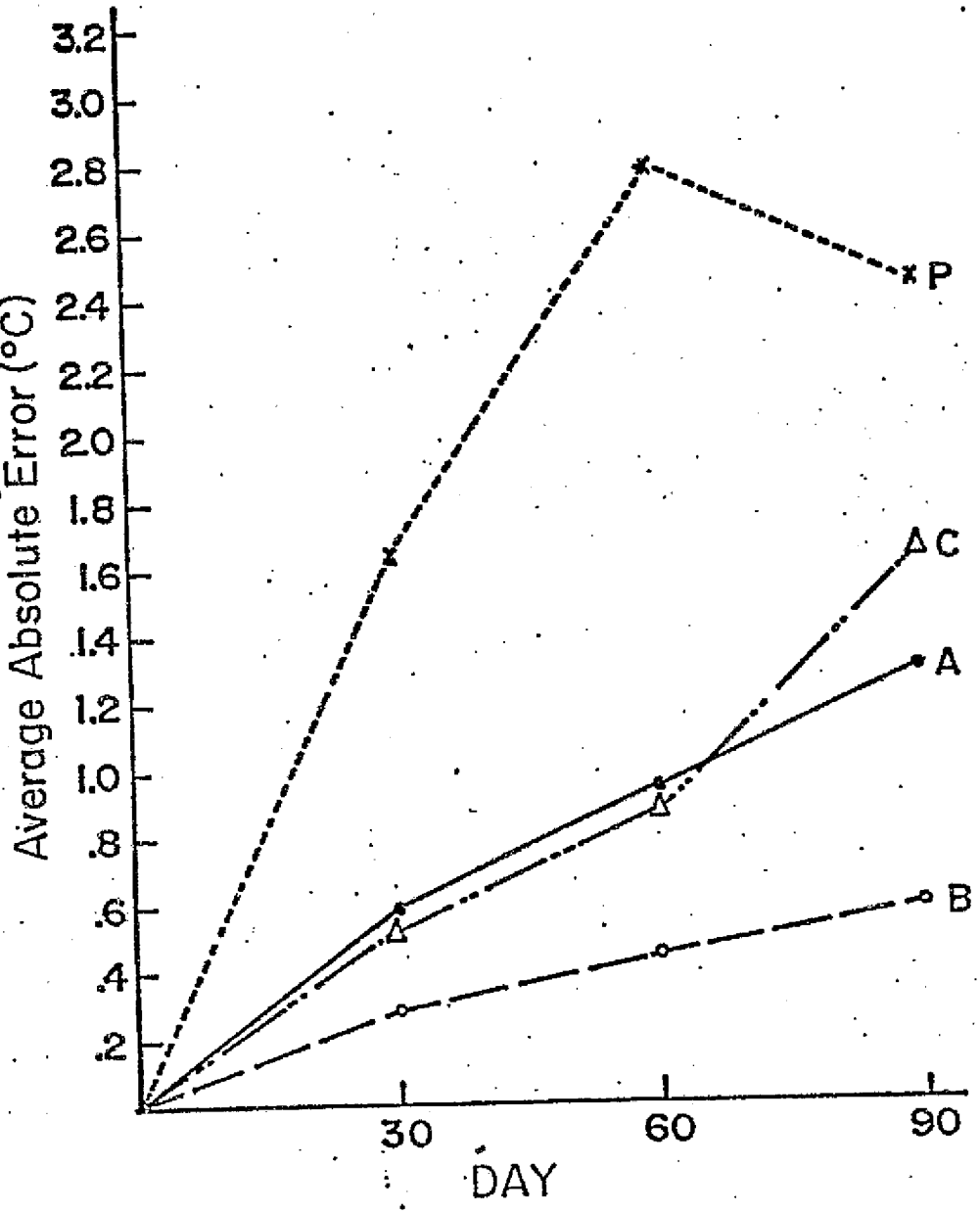

Fig. 15. Same as Fig. 7 for June initial conditions.

versions maintain predictive skill over persistence throughout the ninety period, for both oceans. The advective effect and the effect due to mixed-layer depth changes are considerably larger in this experiment. This is due to the shallower mixed-layer depths and stronger mean currents, as mentioned earlier.

Figures 16 and 17 illustrate the ninety day error fields for versions A and B respectively. From these figures it can be seen that the inclusion of advection has decreased the predictive errors, although they have not been completely eliminated. In the North Atlantic, the predictions at 64% of the gridpoints were improved by advection, while 14% remained the same, and 22% were worsened. In the North Pacific, the inclusion of advection resulted in an improvement at 63% of the gridpoints, while 21% were worsened, and 18% remained unchanged. Once again, the largest advective effects appear to be associated with the major current systems. Too much advection of heat has occurred off the east coast of the United States and in the northern North Atlantic while too little advection has occurred in the northwestern and north-central North Pacific.

Figures 18-21 present the average absolute errors for the four regions, previously defined. These figures show that the average absolute error of the P forecast is consi-

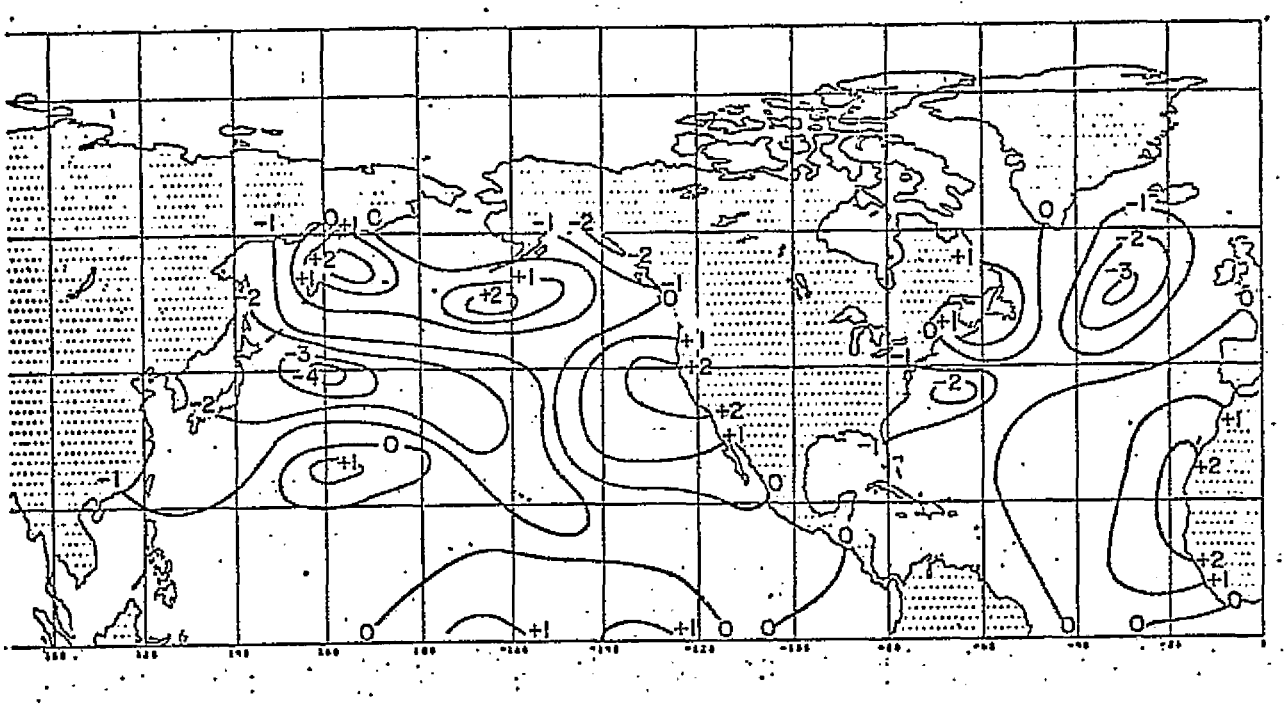

Fig. 16. Same as Fig. 8 for June initial conditions.

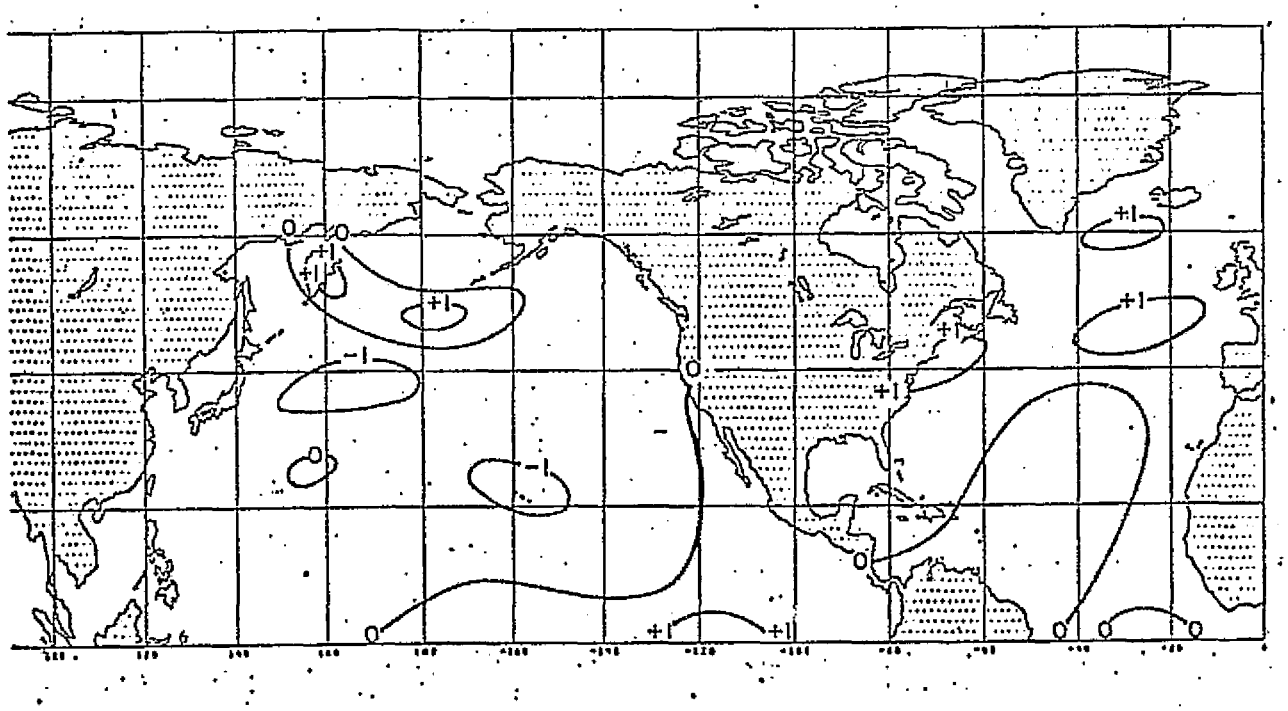

Fig. 17. Same as Fig. 9 for June initial conditions.

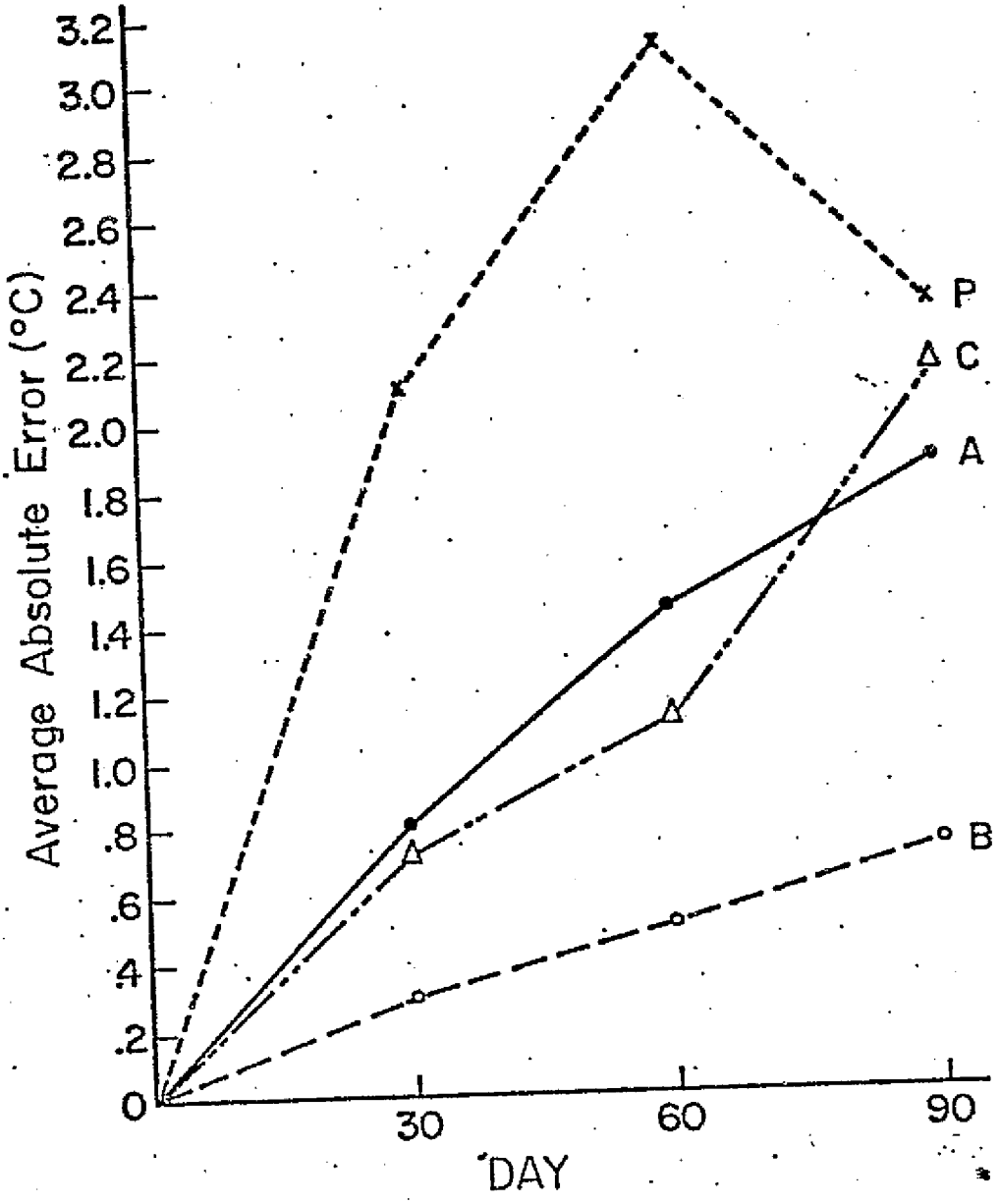

Fig. 18. Same as Fig. 10 for June initial conditions.

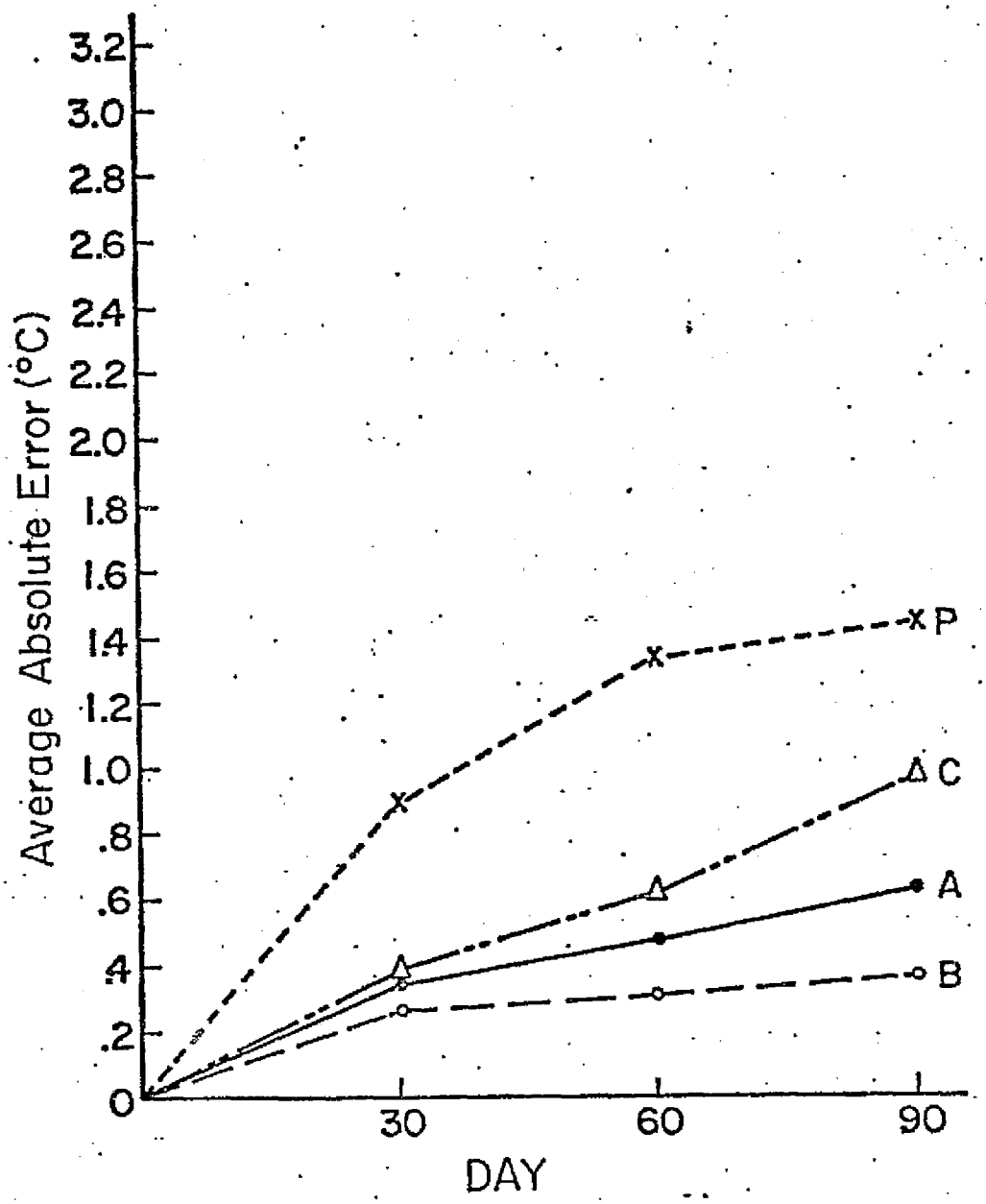

Fig. 19. Same as Fig. 11 for June initial conditions.

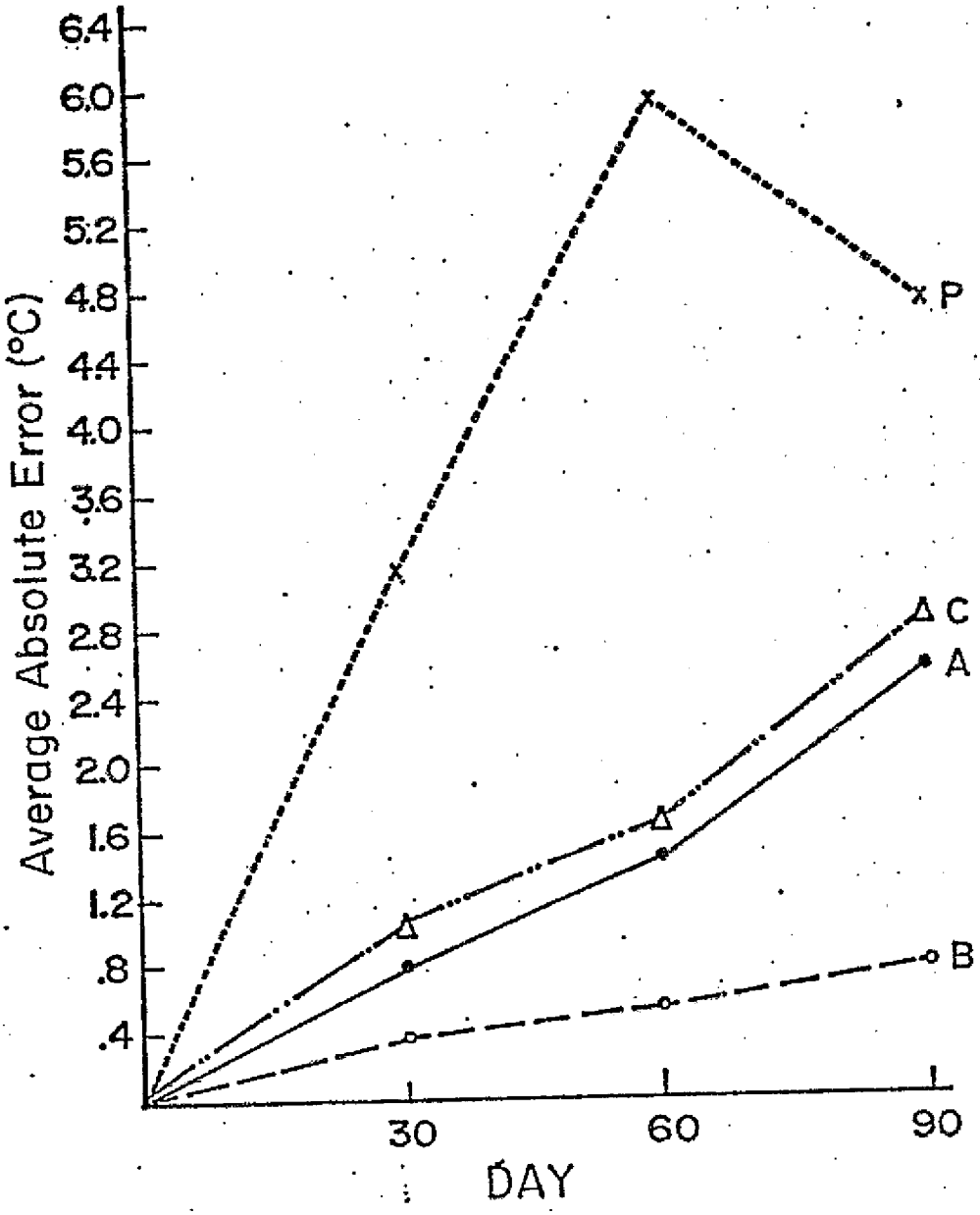

Fig. 20. Same as Fig. 12 for June initial conditions.

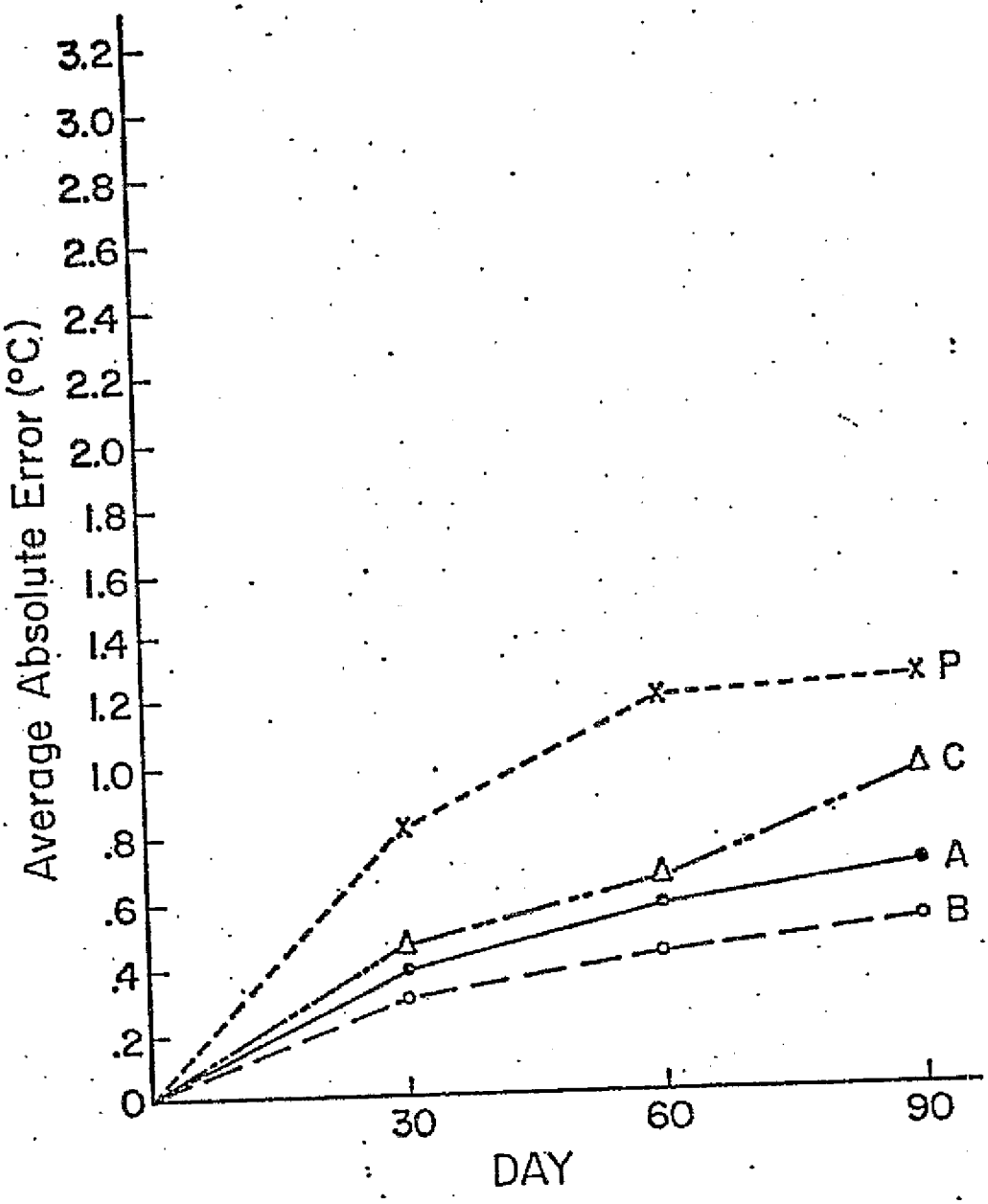

Fig. 21. Same as Fig. 13 for June initial conditions.

derably larger for the northern regions and that this effect is more pronounced in the Pacific Ocean. The advective effect is also considerably larger in the northern regions and the deepening effect is slightly larger than the advective effect in all cases except the thirty and sixty-day predictions for the northern North Atlantic.

5. Anomalous Wind Sensitivity Tests

After the completion of the climatological simulation experiments, several sensitivity tests were conducted to evaluate the role of ocean currents generated by anomalous winds. Specifically, these tests were designed to determine if anomalous advection by such currents could be a major factor in the generation of large scale SST anomalies, as suggested by Namias (1972), and to evaluate the effects of specific anomalous wind patterns. The climatological predictions of the preceding experiments were set up as control runs upon which various hypothetical anomalous winds were superimposed. The sensitivity of the model to these winds was then measured in terms of the difference between the SST predictions of the control run and each test.

Data for this phase of experimentation consisted of exactly the same data fields as described in the preceding section plus the climatological mean wind fields for the cooling season and heating season experiments. The mean zonal and meridional wind components were obtained from the U.S. Navy wind atlas (Chief of Naval Operations 1966). These climatological wind components were specified at each of the secondary gridpoints and remained constant throughout the ninety day predictions. Hypothetical wind components were

also specified at each of the secondary gridpoints and held constant. Wind fields used for these tests were obtained by (A) reversing the climatological wind directions, (B) doubling and (C) halving the wind speeds, (D) doubling and (E) halving the zonal wind components, and (F) doubling and (G) halving the meridional wind components. In additional tests, the major pressure and wind patterns were shifted (H) 12^{o} north, or (I) 12^{o} south, or (J) 10^{o} east or (K) 10^{o} west. Finally (L) the torque on the major anticyclonic gyres of the North Pacific and North Atlantic was reversed. In the latter test, the speed of the westerlies in the $35^{o}N$-$55^{o}N$ band was decreased to 0.1 times its mean value, while the easterlies in the $20^{o}N$-$35^{o}N$ band were decreased to 0.8 times their mean speed and reversed in direction. This wind field is similar to the extreme 1963 winter case in the North Pacific as described by Namias (1970). However, since the climatological SST field was used for this sensitivity test, no attempt was made to simulate the 1963 winter SST anomalies.

The results of these sensitivity tests for the cooling season experiment are presented in Tables 1 and 2. Table 1 presents the average absolute SST differences (^{o}C) computed for the North Atlantic and North Pacific while Table 2 presents the corresponding maximum absolute differences. The tables show that the SST variations due to anomalous wind

Table 1. Average absolute differences in computed sea-surface temperatures (degrees C) from wind sensitivity tests for the cooling season (January initial conditions).

A.) Reversed wind directions	30	60	90 days
North Atlantic	.19	.37	.58
North Pacific	.28	.61	.89
B.) Doubled wind speeds			
North Atlantic	.10	.22	.38
North Pacific	.17	.36	.59
C.) Halved wind speeds			
North Atlantic	.05	.11	.19
North Pacific	.08	.18	.30
D.) Doubled zonal components			
North Atlantic	.13	.26	.42
North Pacific	.19	.37	.57
E.) Halved zonal components			
North Atlantic	.06	.13	.20
North Pacific	.09	.19	.29

Table 1. continued

F.) Doubled meridional components	30	60	90 days
North Atlantic	.08	.17	.28
North Pacific	.09	.19	.32
G.) Halved meridional components			
North Atlantic	.04	.09	.15
North Pacific	.04	.10	.17
H.) 12° northward shift			
North Atlantic	.11	.22	.32
North Pacific	.18	.35	.54
I.) 12° southward shift			
North Atlantic	.10	.19	.33
North Pacific	.12	.30	.51
J.) 10° eastward shift			
North Atlantic	.06	.13	.21
North Pacific	.09	.20	.31
K.) 10° westward shift			
North Atlantic	.06	.12	.22
North Pacific	.09	.19	.31

Table 1. continued

L.) Retarded torque	30	60	90 days
North Atlantic	.10	.20	.33
North Pacific	.16	.30	.45

Table 2. Maximum absolute differences in computed sea-surface temperatures (degrees C) from wind sensitivity tests for the cooling season (January initial conditions).

A.) Reversed wind directions			
North Atlantic	1.3	2.6	4.2
North Pacific	2.2	4.3	6.9

B.) Doubled wind speeds			
North Atlantic	.8	1.7	3.1
North Pacific	1.2	2.6	4.2

C.) Halved wind speeds			
North Atlantic	.4	.8	1.4
North Pacific	.6	1.3	2.0

D.) Doubled zonal components			
North Atlantic	.8	1.6	3.3
North Pacific	1.4	2.8	4.0

Table 2. continued

E.) Halved zonal components	30	60	90 days
North Atlantic	.4	.8	1.7
North Pacific	.7	1.5	2.3

F.) Doubled meridional components			
North Atlantic	.9	2.0	3.1
North Pacific	.9	2.1	3.3

G.) Halved meridional components			
North Atlantic	.4	1.1	1.8
North Pacific	.4	1.2	1.9

H.) 12^{o} northward shift			
North Atlantic	.9	1.8	3.3
North Pacific	1.2	2.2	3.4

I.) 12^{o} southward shift			
North Atlantic	.5	1.2	2.5
North Pacific	.9	2.0	3.1

J.) 10^{o} eastward shift			
North Atlantic	.5	.9	1.6
North Pacific	.8	2.1	3.2

Table 2. continued

K.) 10^{o} westward shift	30	60	90 days
North Atlantic	.5	1.2	1.8
North Pacific	.6	2.1	3.2

L.) Retarded torque			
North Atlantic	.6	1.2	2.3
North Pacific	1.1	2.3	3.5

generated currents can be quite large. In some regions the effect of sustained highly anomalous winds is at least as large as the advective effect due to mean ocean currents.

The largest effect obtained was due to the reversal of the wind circulation. Although such a reversal of winds for the entire North Pacific or North Atlantic is not likely to occur, persistant reversals of the wind over smaller regions have been observed (Namias 1970). Since this apparently represents the maximum effect of anomalous winds, it is useful to look at the regional generation of SST anomalies in the case of reversed winds. The SST difference field after thirty days for this test is presented in Figure 22. Reversal of the winds produces anomalous southerly ocean currents over the northern half of the North Pacific and over the northern and eastern North Atlantic, while anomalous northerly currents are found over the remainder of these oceans. From Figure 22, it can be seen that anomalous warming and cooling associated with these anomalous currents, resulted in several large SST anomalies. Anomalous warming is found along the west coast of California where southeast winds have replaced northwesterly winds, setting up an anomalous southerly current. The largest SST anomaly however is generated in the northwestern North Pacific. A comparison of these differences with those computed from climatological

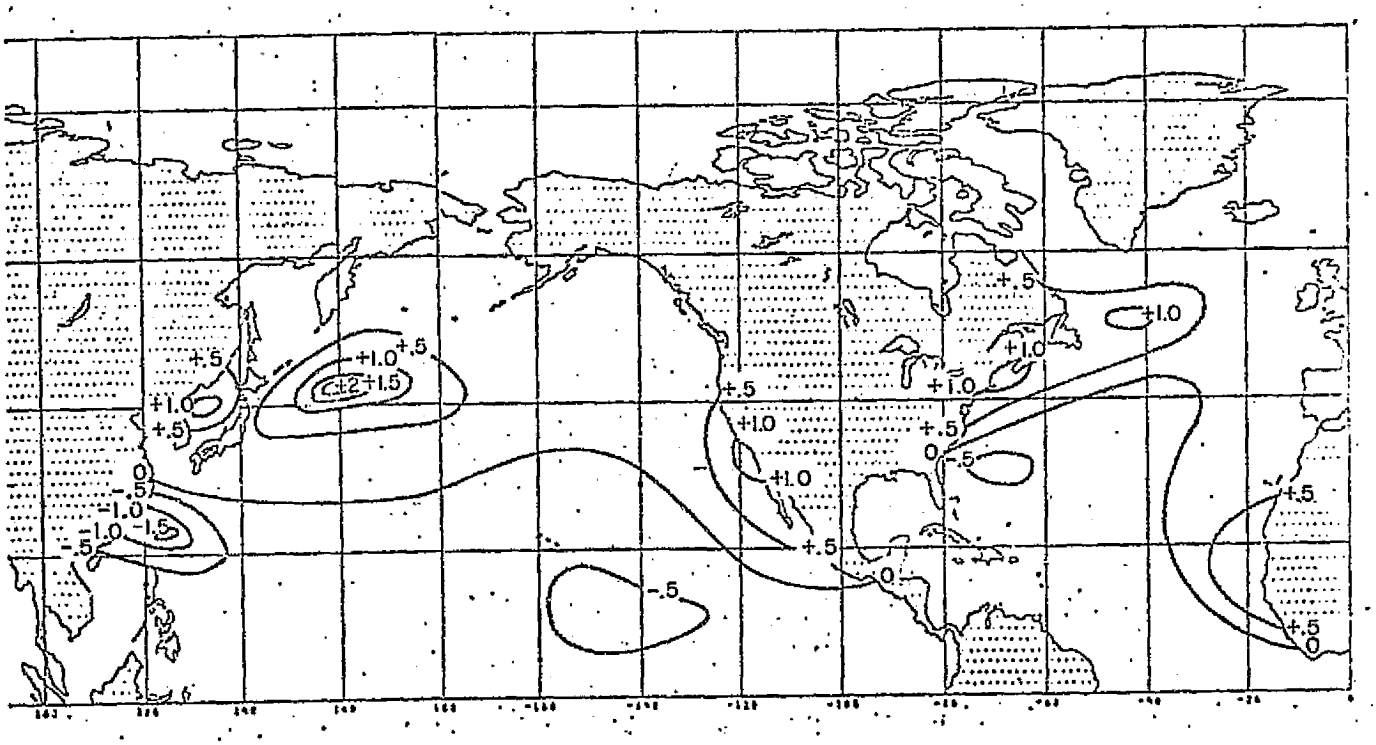

Fig. 22. Sea-surface temperature anomalies (^{o}C) generated after 30-days by reversing the wind directions.

current advection (not reproduced) reveals that this maximum SST anomaly occurs in the region where the strongest westerly current component has been reversed. Further comparison of the difference field with the climatological advection field shows that every large SST anomaly coincides with a correspondingly large wind anomaly. Similar results were obtained for all of the sensitivity tests although the magnitudes of the differences were smaller.

The same set of sensitivity tests was also carried out for the heating season. The summer mean wind field was considerably weaker than the winter field. However, the wind generated currents, when averaged in the mixed layer, were actually slightly stronger in the heating season due to the shallower mixed-layer depths. Tables 3 and 4 present the average and maximum absolute SST differences for this experiment. A comparison of these tables with Tables 1 and 2 reveals that the SST changes due to anomalous wind-generated currents is slightly larger in the heating season than in the cooling season. However this difference is smaller than the difference between the advective effect of mean currents in the two seasons.

Table 3. Average absolute differences in computed sea-surface temperatures (degrees C) from wind sensitivity tests for the heating season (June initial conditions).

	30	60	90 days
A.) Reversed wind directions			
North Atlantic	.24	.47	.66
North Pacific	.31	.64	.95
B.) Doubled wind speeds			
North Atlantic	.12	.26	.42
North Pacific	.20	.39	.61
C., Halved wind speeds			
North Atlantic	.06	.13	.21
North Pacific	.09	.19	.31
D.) Doubled zonal components			
North Atlantic	.14	.29	.45
North Pacific	.19	.41	.63
E.) Halved zonal components			
North Atlantic	.07	.15	.23
North Pacific	.10	.21	.32

Table 3. continued

F.) Doubled meridional components	30	60	90 days
North Atlantic	.10	.21	.33
North Pacific	.13	.26	.41
G.) Halved meridional components			
North Atlantic	.05	.10	.16
North Pacific	.06	.13	.21
H.) 12° northward shift			
North Atlantic	.15	.30	.43
North Pacific	.19	.37	.56
I.) 12° southward shift			
North Atlantic	.14	.27	.40
North Pacific	.17	.35	.53
J.) 10° eastward shift			
North Atlantic	.08	.16	.25
North Pacific	.09	.21	.33
K.) 10° westward shift			
North Atlantic	.09	.18	.28
North Pacific	.10	.22	.35

Table 3. continued

L.) Retarded torque	30	60	90 days
North Atlantic	.15	.30	.43
North Pacific	.20	.38	.57

Table 4. Maximum absolute differences in computed sea-surface temperatures (degrees C) from wind sensitivity tests for the heating season (June initial conditions).

A.) Reversed wind directions

North Atlantic	1.8	3.5	5.4
North Pacific	2.4	4.9	7.8

B.) Doubled wind speeds

North Atlantic	1.0	2.1	3.3
North Pacific	1.3	3.0	4.7

C.) Halved wind speeds

North Atlantic	.5	1.0	1.6
North Pacific	.7	1.5	2.4

D.) Doubled zonal components

North Atlantic	1.1	2.1	3.2
North Pacific	1.4	2.7	4.1

Table 4. continued

E.) Halved zonal components	30	60	90 days
North Atlantic	.6	1.1	1.6
North Pacific	.7	1.3	2.0

F.) Doubled meridional components			
North Atlantic	1.2	2.3	3.5
North Pacific	1.2	2.4	3.7

G.) Halved meridional components			
North Atlantic	.6	1.1	1.8
North Pacific	.6	1.2	1.9

H.) 12^{o} northward shift			
North Atlantic	1.2	2.4	3.5
North Pacific	1.5	2.7	4.0

I.) 12^{o} southward shift			
North Atlantic	.8	1.7	2.7
North Pacific	.9	2.1	3.2

J.) 10^{o} eastward shift			
North Atlantic	.8	1.6	2.3
North Pacific	.8	1.7	2.8

Table 4. continued

K.) 10^{o} westward shift	30	60	90 days
North Atlantic	.6	1.2	2.0
North Pacific	.7	1.3	2.2

L.) Retarded torque			
North Atlantic	1.0	2.1	3.0
North Pacific	1.2	2.5	3.8

6. Synoptic Calculation

In the previous experiments it was demonstrated that the advective mixed-layer model is capable of accounting for the climatological SST changes in the cooling and heating seasons. The sensitivity of the SST predictions to anomalous winds was also shown. In the third phase of experimentation with the model, a thirty day synoptic calculation during the cooling season was performed. This experiment was conducted in order to determine (1) if the inclusion of advection by mean and anomalous currents results in an improvement in the accuracy of the model's synoptic predictions, (2) the magnitude of the advective effect, and (3) the relative importance of advection by mean and anomalous currents.

Data for this experiment were similar to those used in the climatological cooling season experiment, and differed primarily in the use of synoptic SST fields and the inclusion of anomalous winds. Daily observed SST fields were obtained from the U.S. Navy Fleet Numerical Weather Central (FNWC). These are derived from surface ship and buoy observations, supplemented by satellite data, and covered the North Atlantic and North Pacific from 18^{o}N-66^{o}N. Climatological mean winds were obtained from the U.S. Navy

wind atlas (Chief of Naval Operations 1966) while synoptic winds were obtained from the Marine Section of the National Weather Service (NWS) in New York City. These synoptic winds were averaged over the thirty-day period to yield a mean wind field for the month. The climatological values for solar and back radiation, sensible and latent heat fluxes and mixed layer profiles (as described in section 4) were specified at each primary gridpoint, since there were no synoptic observations available for these quantities.

In this experiment, SST predictions were made from January 1, 1974 initial conditions and the mean fluxes were updated daily to drive the model. The mean ocean current values, climatological mean January winds, and mean January 1974 winds were specified at each of the secondary gridpoints and remained constant for the thirty-day period. The anomalous current terms were then computed at each of the secondary gridpoints and added to the mean current value.

SST predictions were made with several different versions of the mixed-layer model in order to evaluate the relative importance of these current terms. Version (A) once again refers to the original version of the GISS ocean model, with no advection included, while Version (B) includes advection by mean currents only. (There was no Version C in this experiment.) Version (D) refers to the case where

advection by both mean and anomalous currents is included. In Version (E) only advection by anomalous currents is considered, and Version (P) is the persistence forecast. In addition, three predictions were computed in which only the advection, and no other model physics was included. Versions (F), (G), and (H) refer to the cases of mean advection, mean and anomalous advection, and anomalous advection respectively. In these latter computations, the thirty-day SST change is due only to the advective effect. The results of all of these predictions were analyzed in terms of the average absolute errors for the North Atlantic and North Pacific and are presented in Table 5.

From this table, it can be seen that the most accurate prediction was produced by model Version D in which the mixed-layer model physics and all current terms have been included. A comparison of Versions A, B, D, and E reveals that (1) the improvement of accuracy due to the inclusion of mean currents is small, (2) a much larger improvement results when all current terms are included, and (3) the improvement of the predictions due to advection by anomalous currents is more important than the improvement due to mean currents in this experiment. A comparison of Versions F, G, H and P reveals that the anomalous current alone yield the most accurate predictions. All model

Table 5. Average absolute error, ^{o}C, in the thirty-day SST predictions from January 1, 1974 initial conditions.

	Version	North Atlantic	North Pacific
Mixed-Layer Physics plus			
No Advection	A	.75	.71
Mean Advection	B	.70	.68
Complete Model	D	.57	.59
Anomalous Advection	E	.66	.64
No Mixed Layer Physics			
Mean Advection	F	.88	.95
Total Advection	G	.84	.87
Anomalous Advection	H	.82	.79
Persistance	P	.96	.89

versions maintain skill over persistence with the exception of Version F for the North Pacific.

In order to gain further insight into the importance of advection by anomalous currents, the maps of mean sea level pressure for January 1974, predicted anomalous SST change due to anomalous advection (Version H), and observed anomalous SST changes are presented in Figures 23-25. Figure 23 shows the isobars of average sea level pressure for January 1974. In the North Atlantic, the mean circulation was dominated by an intense Icelandic low. This low was centered close to its normal position but had a central pressure 22 millibars (mb.) deeper than normal. The subtropical high pressure belt in the North Atlantic was close to its normal position and had a central pressure only 1 mb. higher than normal. In the North Pacific, the western lobe of the Aleution low was dominant in January 1974 and was 4 mb. deeper than normal. Meanwhile the eastern North Pacific high was centered slightly further east than normal and had a central pressure 4 mb. lower than normal.

The predicted and observed anomalies of thirty-day SST change are presented in Figures 24 and 25. A comparison of these fields reveals that there is a remarkable qualitative agreement between the two fields. Almost all of the major areas of anomalous SST change have been predicted.

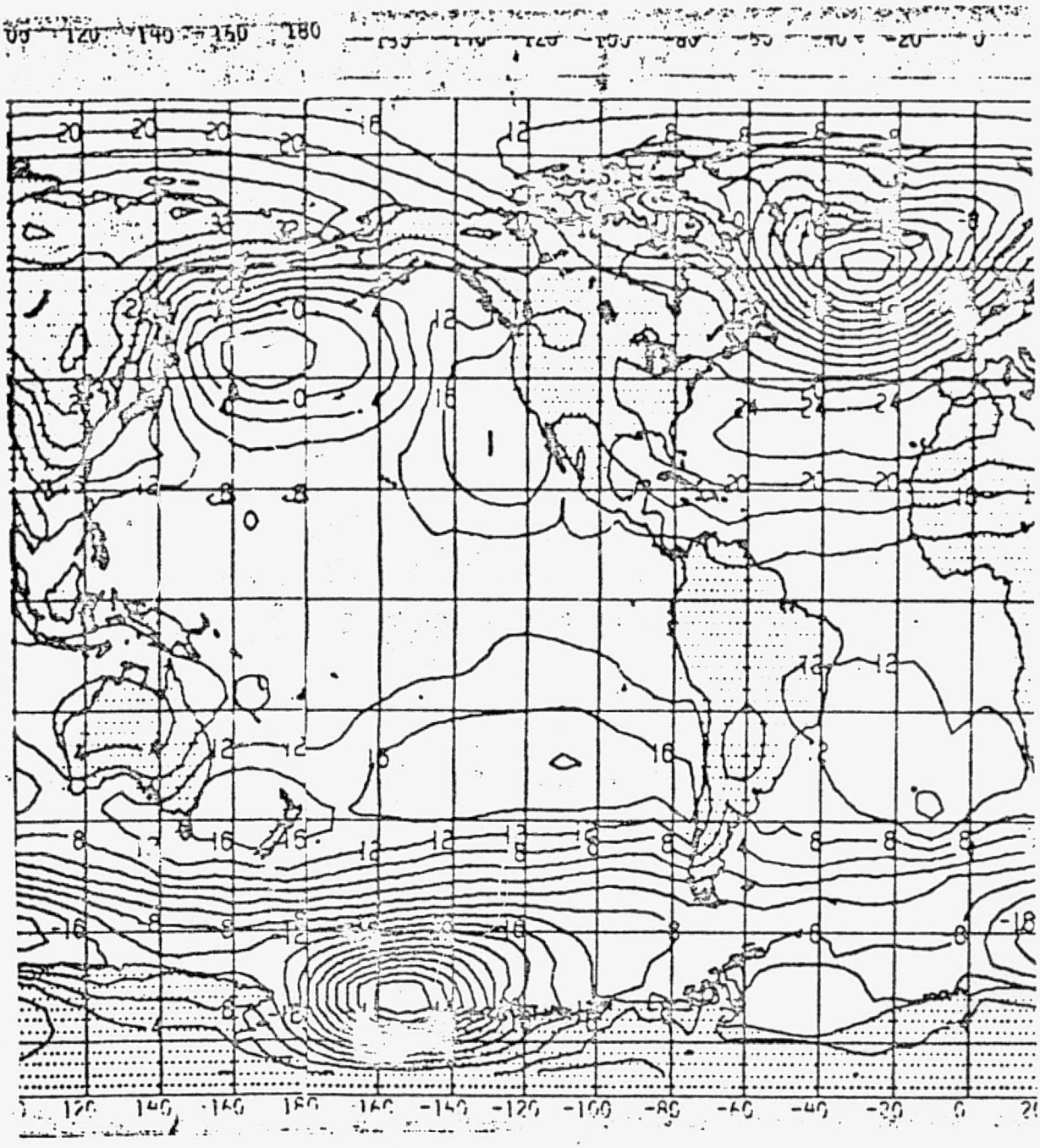

Fig. 23. Mean sea level pressure pattern (mb.) for January 1974.

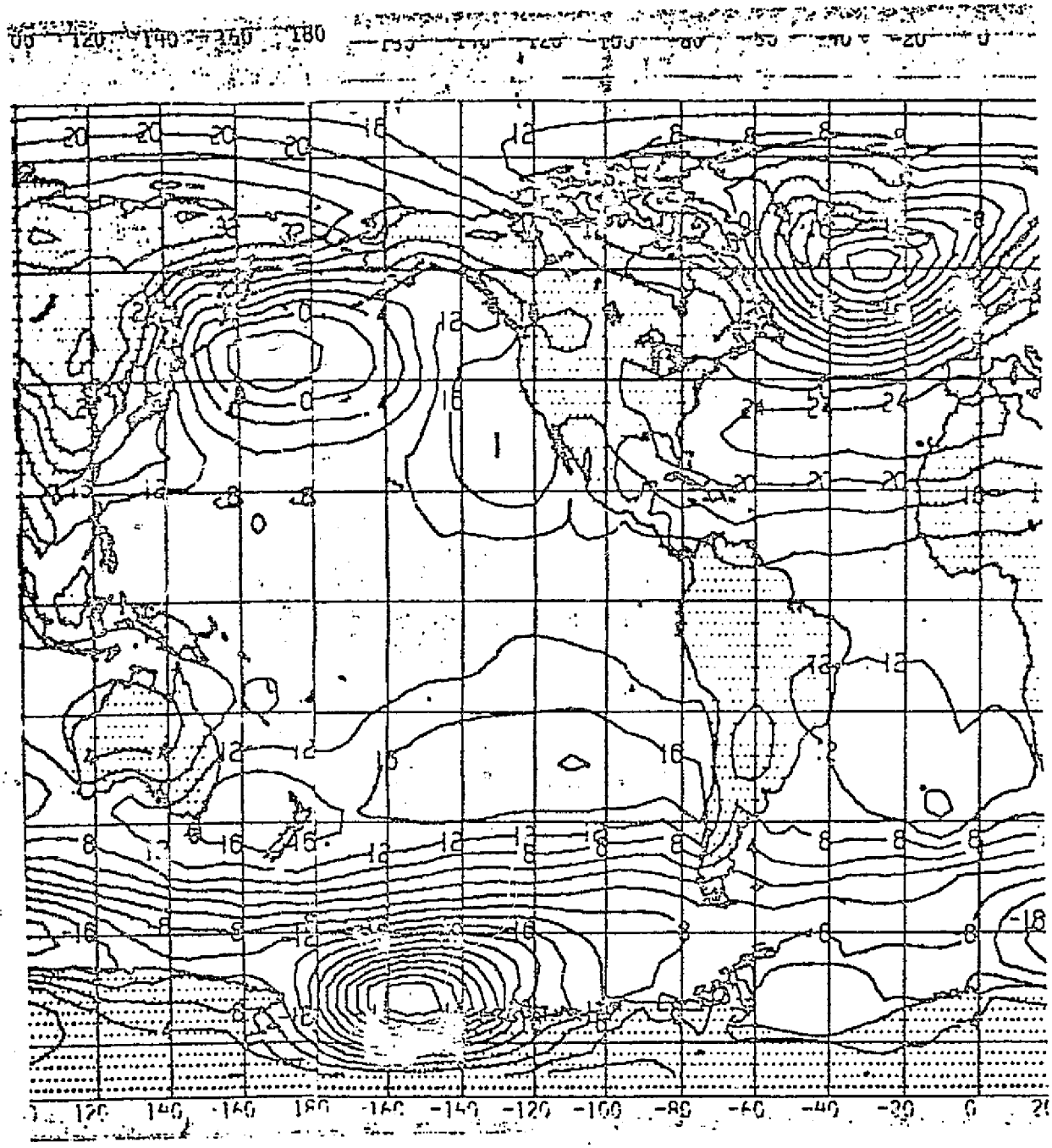

Fig. 23. Mean sea level pressure pattern (mb.) for January 1974.

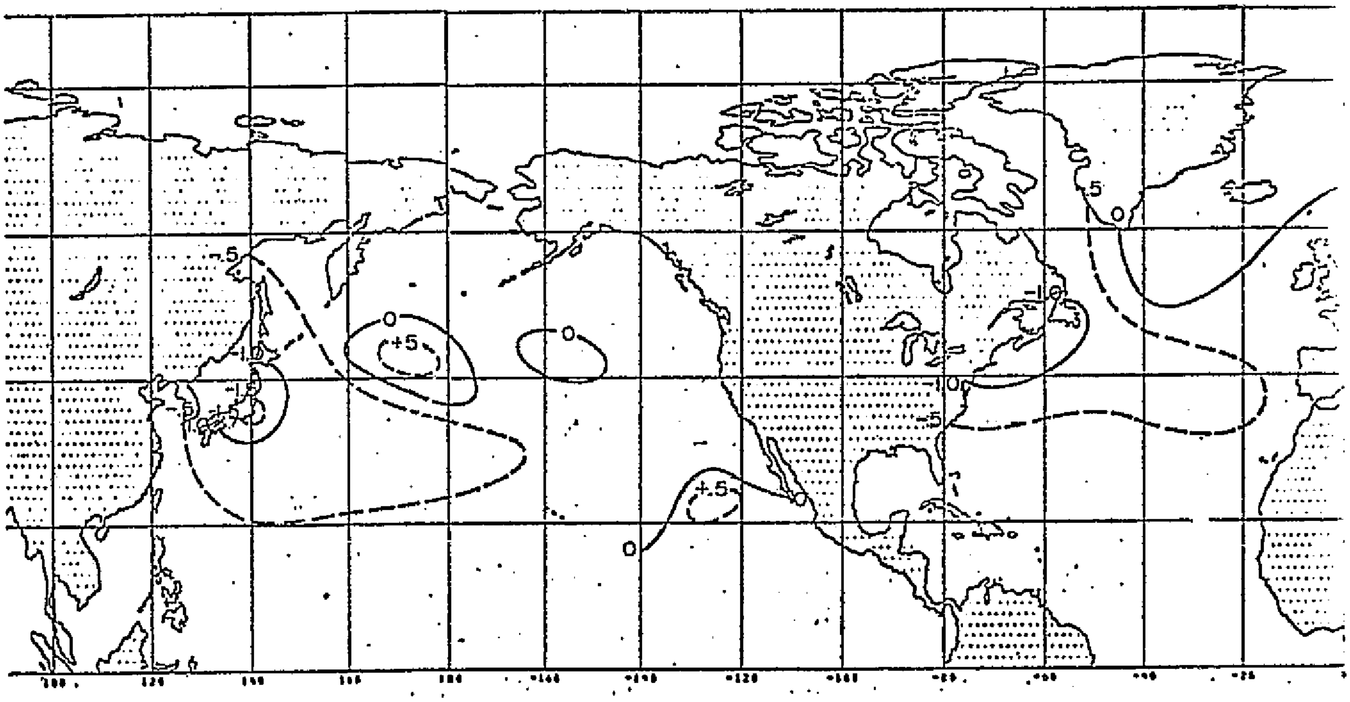

Fig. 24. Predicted changes of sea-surface temperatures (°C) from January 1 to January 31, 1974 using model version H.

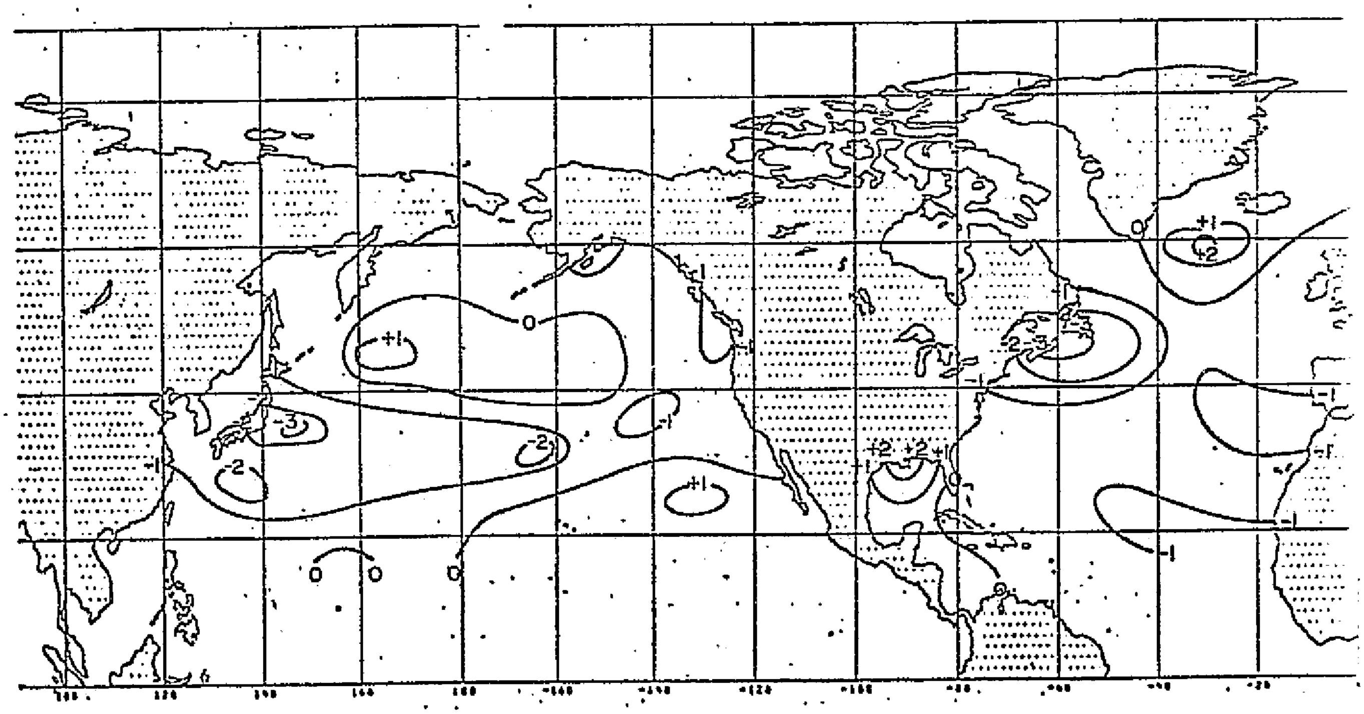

Fig. 25. Observed anomalous changes of sea-surface temperature (°C) from January 1 to January 31, 1974.

However, the magnitude of the advective anomalies is in most cases less than half of the observed anomalous change. This indicates that although anomalous advection was important it was not dominant in January 1974.

7. Summary and Conclusions

By eliminating the assumption of horizontal homogeneity and superimposing a mean and anomalous wind driven current field, the effects of horizontal advection of heat have been incorporated into an existing, two-dimensional, time-dependent ocean mixed-layer model. Mixed-layer depths and temperatures in the North Atlantic and North Pacific Oceans have been computed with the model by means of a numerical scheme which separates the calculation into advective and nonadvective parts. This approach allows the original mixed-layer model to account for the effects of solar and back radiation, sensible and latent heat exchange with the atmosphere, and mixed-layer depth changes at each point, while the superimposed current field serves to couple the gridpoints through the advection of heat and mass.

Three phases of experimentation have been conducted with this model. In Section 4, the model's ability to account for climatological SST variations was evaluated through two experiments - one in the cooling season and one in the heating season. These experiments showed that (1) the inclusion of advection results in a marked improvement in the accuracy of the ocean model climatology, (2) the largest advective effects are associated with the major

current systems, (3) the advective effect is larger in the heating season than in the cooling season, and (4) the advective effect and the effect due to mixed-layer depth variations are of similar magnitude.

In Section 5, the sensitivity of the model SST predictions to various hypothetical anomalous wind distributions was evaluated. The results of this phase of experimentation indicate that the ocean model (and presumably the real ocean as well) responds sensitively to anomalous winds, and that sustained highly anomalous winds are capable of generating large-scale SST anomalies. The largest SST anomalies resulted from sustained reversals of the wind direction.

The results of a single synoptic calculation during the cooling season were presented in Section 6. This calculation showed that the inclusion of mean and anomalous advection resulted in an improvement of the accuracy of the model's SST predictions. However, for the case studied, mean fluxes were used to drive the model and the anomalous currents were computed using observed rather than predicted winds. In order to determine the model's usefulness for predicting real time SST variations, predicted fluxes and winds must be used, and therefore the model should be coupled to a predictive atmospheric model for this purpose.

The study has demonstrated the importance of horizontal advection in an ocean mixed-layer model. In coupling a mixed-layer ocean model to an atmospheric general circulation or numerical weather prediction model, it is clearly desirable that horizontal advection be included in the ocean as well as in the atmosphere, if the coupled model is to be useful for extended and long-range prediction. It is also apparent, however, that over a period of the order of one month or more, errors in the predicted surface wind fields may generate errors in the SST fields, which could result in a positive feedback of error into the atmospheric prediction. Planned experiments with a coupled ocean-atmosphere model should help to determine how serious this problem is likely to be with presently available models.

References

Adem, J., 1970: On the prediction of mean monthly ocean temperatures. Tellus, 22, 410-430.

Arthur, R.S., 1966: Estimation of mean monthly anomalies of sea-surface temperature. Journal of Geophysical Research, 71, 2689-2690.

Bathen, K.H., 1971: Heat storage and advection in the North Pacific Ocean. Journal of Geophysical Research, 76, 676-687.

Bjerknes, J., 1966: A possible response of the atmospheric Hadley circulation to equatorial anomalies of ocean temperature. Tellus, 18, 820-829.

_____, 1969: Atmospheric teleconnections from the equatorial Pacific. Monthly Weather Review, 97, 163-172.

Bryan, K., 1969: Climate and the ocean circulation III. The ocean model. Monthly Weather Review, 97, 806-827.

_____, 1975: Three dimensional numerical models of the ocean circulation. pp. 94-106 in Numerical Models of Ocean Circulation, National Academy of Sciences, Washington, D.C., 364 pp.

Chief of Naval Operations, 1966: Components of the 1000-mb. Winds (or Surface Winds) of the Northern Hemisphere. NAVAIR 50-1C-51. Naval Weather Service Command, Washington, D.C.

Clark, N.E., 1972: Specification of sea-surface temperature anomaly patterns in the eastern North Pacific. Journal of Physical Oceanography, 2, 391-404.

Cox, M.D., 1975: A baroclinic numerical model of the world ocean: Preliminary results. pp. 107-120 in Numerical Models of Ocean Circulation. National Academy of Sciences, Washington, D.C., 364 pp.

Defant, A.D., 1961: Physical Oceanography. Vol. 1. Pergamon, New York, 729 pp.

Denman, K.L., 1973: A time-dependent model of the upper ocean. Journal of Physical Oceanography, 3, 173-184.

_____, and M. Miyake, 1973: Upper layer modification at ocean station "Papa" : Observations and Simulation. Journal of Physical Oceanography, 2, 185-196.

Druyan, L.M., R.C.J. Sommerville and W.J. Quirk, 1975: Extended-range forecasts with the GISS model of the global atmosphere. Monthly Weather Review, 103, 779-795.

Eber, L.E., 1961: Effects of wind-induced advection on sea surface temperature. Journal of Geophysical Research, 66, 839-844.

Ekman, V.W., 1905: On the influence of the earth's rotation on ocean currents. Arkiv for Matematik, Astronomi och Fysik, 2, No. 11.

Hammond, A.L., 1974: Long-range forecasting: Sea temperature anomalies. Science, 184, 1064-1065.

Houghton, D.D., J.E. Kutzbach, M.McClintock and D. Suchman, 1974: Response of a general circulation model to a sea temperature perturbation. Journal of the Atmospheric Sciences, 31, 857-868.

Jacob, W.C., 1967: Numerical semiprediction of monthly mean sea-surface temperature. Journal of Geophysical Research, 72, 1681-1689.

Jastrow, R. and M. Halem, 1973: Accuracy and coverage of temperature data derived from the IR radiometer on the NOAA2 satellite. Journal of the Atmospheric Sciences, 30, 958-964.

Kato, H. and O.M. Phillips, 1969: On the penetration of a turbulent layer into a stratified fluid. Journal of Fluid Mechanics, 37, 643-655.

Kraus, E.B. and J.S. Turner, 1967: A one-dimensional model of the seasonal thermocline: II. The general theory and its consequences. Tellus, 19, 98-106.

Kurihara, Y. and J.L. Holloway, Jr., 1967: Numerical integration of a nine-level global primitive equations model formulated by the box method. Monthly Weather Review, 95, 509-530.

Miller, J.R., 1973: A mixed-layer ocean model for medium-range forecasting. GISS Research Review, NASA, 100.

_____, 1974: The GISS ocean model. GISS Research Review, NASA, 32-35.

_____, 1975: (Personal communication)

Munk, W.H. and E.R. Anderson, 1948: Notes on a theory of the thermocline. Journal of Marine Research, 7, 276-295.

Namias, J., 1959: Recent seasonal interactions between North Pacific Waters and the overlying atmospheric circulation. Journal of Geophysical Research, 64, 631-646.

_____, 1968: Long-range forecasting of the atmosphere and its oceanic boundary - An interdisciplinary problem. California Marine Research Commission, 29-42.

_____, 1969: Seasonal interactions between the North Pacific Ocean and the atmosphere during the 1960's. Monthly Weather Review, 97, 173-192.

_____, 1970: Macroscale variations in sea-surface temperatures in the North Pacific. Journal of Geophysical Research, 75, 565-582.

_____, 1971: The 1968-69 winter as an outgrowth of sea and air coupling during antecedent seasons. Journal of Physical Oceanography, 1, 65-81.

_____, 1972: Experiments in Objectively Predicting some atmospheric and oceanic variables for the wind of 1971-72. Journal of Applied Meteorology, 11, 1164-1174.

_____, 1973: Thermal communication between the sea surface and lower troposphere. Journal of Physical Oceanography, 3, 373-378.

_____, 1974: Longevity of a coupled air-sea continent system. Monthly Weather Review, 102, 638-648.

Neumann, G., 1968: Ocean Currents. London, 352 pp.

_____, and W.J. Pierson, 1966: Principles of Physical Oceanography. Prentice Hall, Englewood Cliffs, 545 pp.

Niiler, P.P., 1973: Deepening of the wind-mixed layer. Unpublished manuscript. 29 pp.

Phillips, O.M., 1966: The Dynamics of the Upper Ocean. Cambridge University, London, 261 pp.

Pollard, R.T., P.G. Rhines and R.R.Y. Thompson, 1973: The deepening of the wind-mixed layer. Journal of Geophysical Fluid Mechanics, 3, 381-404.

Rao, P.K., 1974: An evaluation of May 1971 satellite-derived sea-surface temperatures for the Southern Hemisphere. NOAA Technical Report NESS 69, Washington, D.C., 13 pp.

_____, W.L. Smith and R. Koffler, 1972: Global sea-surface temperature distribution determined from an environmental satellite. Monthly Weather Review, 100, 10-14.

Rowntree, P.R., 1972: The influence of tropical East Pacific Ocean temperatures on the atmosphere. Quarterly Journal of the Royal Meteorological Society, 98, 290-321.

Saur, J.F.T., 1963: A study of the quality of sea water temperature reported in logs of ship's weather observations. Journal of Applied Meteorology, 2, 417-425.

Schutz, C. and W.L. Gates, 1971: Global Climatic Data for Surface, 800 mb, 400 mb, R-915-ARPA, Rand Corporation, Santa Monica, 173 pp.

Seidman, A.N., 1975: Numerical experiments on long-range weather prediction. Ph.D. thesis, Columbia University (unpublished), 123 pp.

Smith, W.L., D.T. Hilleary, J.C. Fisher, H.B. Howell and H.M. Woolf, 1974: Nimbus-5 ITPR experiment. Applied Optics, 13, 499-506.

Sommerville, R.C.J., P.H. Stone, M. Halem, J.E. Hansen, J. S. Hogan, L.M. Druyan, G. Russell, A.A. Louis, W. J. Quirk and J. Tenenbaum, 1974: The GISS model of the global atmosphere. Journal of the Atmospheric Sciences, 31, 84-117.

Spar, J., 1973: Some effects of surface anomalies in a global general circulation model. Monthly Weather Review, 101, 91-100.

____, and R. Atlas, 1975: Atmospheric response to variations in sea-surface temperature. Journal of Applied Meteorology, 14, 1235-1245.

____, R. Atlas and E. Kuo, 1975: A 30 day forecast experiment with the GISS model and updated sea-surface temperatures. (unpublished) 23 pp.

Stommel, H., 1965: The Gulf Stream - A Physical and Dynamical Description. University of California, Berkeley and Los Angeles, and Cambridge University, London, 248 pp.

_____ and K. Yoshida, 1972: Kuroshio Physical Aspects of the Japan Current. University of Washington, Seattle and London, 517 pp.

Sverdrup, H.O., M.W. Johnson and R.H. Fleming, 1942: The Oceans - Their Physics, Chemistry and General Biology. Prentice Hall,

Takano, K., 1975: A numerical simulation of the world ocean circulation: Preliminary results. pp. 121-132 in Numerical Models of Ocean Circulation National Academy of Sciences, Washington, D.C., 364 pp.

Turner, J.S. and E.G. Kraus, 1967: A one-dimensional model of the seasonal thermocline. I. A laboratory experiment and its interpretation. Tellus, 19, 88-97.

U.S. Weather Bureau and U.S. Navy Hydrographic Office, 1959: Climatological and Oceanographic Atlas for Mariners. Vol. I., Washington, D.C., 6 pp.

U.S. Weather Bureau and U.S. Navy Hydrographic Office, 1961: Climatological and Oceanographic Atlas for Mariners. Vol. II., Washington, D.C., 5 pp.

Washington, W.M. and L.G. Thiel, 1970: Digitized monthly mean ocean temperatures over the globe, NCAR Technical Note 54, Boulder, 30 pp.